# THE GENERALISED FINITE ELEMENT METHOD AND ELECTRO-MAGNETIC PROBLEMS

O. C. ZIENKIEWICZ

University College of Swansea, U.K.

## ABSTRACT

The paper deals with a generalised presentation of the finite element method as a weighted residual (weak) process which as special cases can include the "standard" finite element method with piecewise polynomial approximations, the finite difference method and boundary integral equation procedures. It is shown how in one formulation the advantages of each of these sub-classes can be utilised and further how the coupling can be executed in a symmetric mode. The paper concludes with a short discussion of application to magneto-static problems and throughout the paper the Poisson equation is used as an illustrative example.

## 1. INTRODUCTION

The finite element method which originated from the needs of structural engineers is today identified as a very general process of approximation applicable to a variety of problems dealing with continua. With some generalisation of the definition the method can be considered to embrace in addition to the "standard" finite element process in which piecewise polynomial approximations are taken, such classical procedures as the finite difference method and boundary solution methods. A number of texts written in recent years deal effectively with the mathematics and practicalities of the approach. In this paper we try to focus and extend the generality so that a fuller understanding is available. (1)-(3)

In recent years several developments have taken place in the fields of structural and fluid mechanics which enlarge the scope of the method. These are quite generally applicable in other areas and can therefore be of immediate benefit in the special problem of magneto-statics. Two of such areas are of particular importance elsewhere:

(a) the use of reduced (inexact) numerical integration to improve the accuracy of the approximation (viz. ref. 3 Chapter 11)

and

(b) the combination of standard finite element processes with boundary solution methods (4) which are particularly effective in dealing with exterior, infinite, domains such as are typical of magneto-static situations. Indeed in this context another development, i.e. that of "infinite elements" is a particular possibility (5) (viz. Ref. 3 Chapter 23).

In this paper we shall concentrate on expanding the general basis of the finite element method and will illustrate some of the concepts introduced by the Poisson equation of the form

$$\nabla \underset{\sim}{k} \nabla \phi - p = 0 \tag{1}$$

which is typical of many magneto-static problems. Indeed in last section we shall return to this particular application and show how it arises in the formulation.

## 2. THE GENERALISED FINITE ELEMENT DEFINITION

To set the stage we shall concentrate on the approximate solution of a continuum problem involving the determination of a function (Fig. 1) such that

$$A(\phi) = 0 \qquad \text{in a domain } \Omega \tag{2a}$$

and

$$\bar{B}(\phi) = 0 \qquad \text{on the boundary part } \Gamma_1$$

$$\bar{\bar{B}}(\phi) = 0 \qquad \text{— " — } \Gamma_2 \tag{2b}$$

In the above $A$ and $B$ can be linear or non-linear operators of a differential or indeed, integral type.

The generalised finite element method will be defined as an approximation in which:

(A) The independent varinble $\phi$ is expanded in a finite series

$$\phi \approx \hat{\phi} = N_i a_i \qquad i = 1-n \tag{3}$$

(repeated index implying a summation).

In above,

$$N_i = N_i(\underset{\sim}{x}) \tag{4}$$

where $\underset{\sim}{x}$ are the independent coordinates and $N_i$ are prescribed functions known alternatively as shape, basis or trial functions. $a_i$ are a set of parameters determining the approximate solution.

(B) The algebraic equations for numerical determination of the solution parameters are formed as

$$\int_\Omega W_j A(\hat{\phi})\, d\Omega + \int_{\Gamma_1} \bar{W}_j \bar{B}(\hat{\phi})\, d\Omega + \int_{\Gamma_2} \bar{\bar{W}} \bar{\bar{B}}(\hat{\phi})\, d\Omega = Q_{(5)}$$

where $W_j$, $\bar{W}_j$ and $\bar{\bar{W}}_j$ etc. are a set $j = 1-n$ of independent weighting (or test) functions.

It follows immediately that the algebraic equations can be assembled by evaluating the various integrals for sub-domains $\Omega^e$ (and $\Gamma_1^e$ etc.) such that

$$\Omega = \sum \Omega^e \qquad \Gamma_1 = \sum \Gamma_1^e \qquad etc \tag{6}$$

and adding the contributions. This is a corollary of the simple fact that

$$\int_{\Omega} (\ ) d\Omega \equiv \sum_{e=1}^{n} \int_{\Omega^e} (\ ) d\Omega \tag{7}$$

and means that the equations of approximation behave as a "standard discrete system" and obey its general rules (these indeed are often identified with simple physical concepts of which the Kirchhoff's equations for circuits are a particular case).

For linear systems equations (5) result in a matrix equation

$$\underset{\sim}{H}\,\underset{\sim}{a} = \underset{\sim}{f} \tag{8}$$

which can be solved in a variety of ways which we do not need here to discuss.

In conventional finite element analysis the parameters $\underset{\sim}{a}$ are often identified with the values of $\phi$ at nodes i and the shape functions $N_i$ have a narrow base being defined separately in each element. This leads to banded forms of equation (8) and is particularly useful in solution but by no means essential.

Equation (5) can be interpreted as an exact statement equivalent to equation (2) as it is true for all functions $W_i$, $\bar{W}_i$ and $\bar{W}$ and also for the exact form of $\phi$. It follows therefore that the process is convergent providing

(a) the set of expansion functions (3) is complete, i.e. can represent the exact solution when $n \to \infty$

(b) integrals of equation (5) can be evaluated at all points

and

(c) suitably independent sets of $W$ are taken.

We shall not discuss in detail the requirements imposed by above on the choice of shape functions. These can be found elsewhere (1-3). It is however, important to note that

(i) order of continuity may be reduced by integration by parts of the domain integrals.

(ii) the generality of the formulation is not reduced if $\bar{W}$ and $\bar{\bar{W}}$ are taken as arbitrary, non-zero functions of $W$. This is important, reducing the need for separate choices.

In certain cases it is possible to eliminate some of the boundary integrals involving the unknown $\phi$ by a suitable choice of $\bar{W}$. Corresponding boundary conditions are then referred to as natural.

## 3. ILLUSTRATION

Consider equations

$$\begin{aligned} A(\phi) &\equiv \underset{\sim}{\nabla}^T k \underset{\sim}{\nabla}\phi - p = 0 && \underset{\sim}{x} \in \Omega \\ \bar{B}(\phi) &\equiv k\frac{\partial\phi}{\partial n} - \bar{q} = 0 && \underset{\sim}{x} \in \Gamma_1 \\ \bar{\bar{B}}(\phi) &\equiv \phi - \bar{\phi} = 0 && \underset{\sim}{x} \in \Gamma_2 \end{aligned} \tag{9}$$

The weighted form of equation (5) in this case becomes

$$\int_{\Omega} W_i (\underset{\sim}{\nabla}^T k \underset{\sim}{\nabla}\hat{\phi} - p)\, d\Omega + \int_{\Gamma_1} \bar{W}_i \left(\frac{\partial\hat{\phi}}{\partial n} - \bar{q}\right) d\Gamma + \int_{\Gamma_2} \bar{\bar{W}} (\hat{\phi} - \bar{\phi})\, d\Gamma = 0 \tag{10}$$

Integration by parts (Green's theorem) of the first term gives

$$-\int_{\Omega} \underset{\sim}{\nabla}^T W_i \cdot k \underset{\sim}{\nabla}\hat{\phi}\, d\Omega + \int_{\Gamma_1+\Gamma_2} W_i \frac{\partial\hat{\phi}}{\partial n} d\Gamma \tag{11}$$

and if we choose $\bar{W}_i = -W_i$ the normal gradient term disappears in the integral along $\Gamma_1$ giving

$$\int_{\Omega} \underset{\sim}{\nabla} W_i \cdot k \underset{\sim}{\nabla}\hat{\phi}\, d\Omega + \int_{\Omega} W_i p\, d\Omega - \int_{\Gamma_1} W_i \bar{q}\, d\Gamma + \int_{\Gamma_2} W_i \frac{\partial\hat{\phi}}{\partial n} d\Gamma - \int_{\Gamma_2} \bar{\bar{W}} (\hat{\phi} - \bar{\phi})\, d\Gamma = 0 \tag{12}$$

This shows that the first boundary conditions here assumed was "natural".

On substitution of expansion (3) we have a system of linear equations of the form

$$\underset{\sim}{H}\,\underset{\sim}{a} = \underset{\sim}{f}$$

with

$$H_{ji} = \int_{\Omega} \underset{\sim}{\nabla} W_j \underset{\sim}{k} \underset{\sim}{\nabla} N_i \, d\Omega + \int_{\Gamma_2} W_j \frac{\partial N_i}{\partial n} \, d\Gamma - \int_{\Gamma_2} \bar{W}_j \, N_i \, d\Gamma \tag{13a}$$

and

$$f_j = -\int_{\Omega} W_j \, p + \int_{\Gamma_1} W_j \, \bar{q} \, d\Gamma - \int_{\Gamma_2} \bar{W}_j \, \bar{\phi} \, d\Gamma \tag{13b}$$

Many choices can be made for $W_j$ and $\bar{W}_j$ in solution but it is very desirable to obtain symmetric matrices (showing a variational origin of the equation and leading to a cheaper solution (3)). In the above example this is simply achieved by the following choice

$$W_j = N_j$$
$$\bar{W} = \frac{\partial N_j}{\partial n} \tag{14}$$

The symmetric form of approximation which we have obtained is equivalent to a certain mixed variational principle (3). In many cases but by no mans generally, it is possible to enforce the second boundary condition explicitly and thus eliminate it. This in fact is generally done in the "standard finite element process".

## 4. RELATIONSHIP WITH OTHER APPROXIMATIONS. FINITE DIFFERENCE AND BOUNDARY SOLUTIONS

It can be shown that the choice

$$W_j = \delta(\underset{\sim}{x}_j) \tag{15}$$

where $\delta(\underset{\sim}{x}_j)$ is the Dirac delta function and where suitably localised shape functions are used the standard finite difference approximation is obtained. Thus this approximation can readily be shown to be included in the general formulation.

On the other hand if we limit our considerations to linear operators

$$A(\phi) \equiv L\phi = 0$$

and choose shape functions such that

$$L N_i = 0 \qquad \underset{\sim}{x} \in \Omega \tag{16}$$

then the domain part of the integral in expression (5) disappears and we have only now to satisfy the boundary conditions. The general approximation form is now given by

$$\int_{\Gamma_1} \bar{W}_j \, \bar{B} \hat{\phi} \, d\Gamma + \int_{\Gamma_2} \bar{\bar{W}}_j \, \bar{\bar{B}} \hat{\phi} \, d\Gamma = 0 \tag{17}$$

which reduces again on approximation to

$$\underset{\sim}{H}\,\underset{\sim}{a} = \underset{\sim}{f} \tag{18}$$

Here the coefficients of $\underset{\sim}{H}$ only involve boundary terms. Such form of approximations was first introduced by Trefftz and forms a very important sub-class.(6)

Illustration

For the special case considered in equation (9) the boundary form of approximation is

$$\int_{\Gamma_1} \bar{W}_j \left( \frac{\partial \hat{\phi}}{\partial n} - \bar{q} \right) d\Gamma + \int_{\Gamma_2} \bar{\bar{W}}_j \left( \hat{\phi} - \bar{\phi} \right) = 0 \tag{19}$$

and

$$H_{ji} = \int_{\Gamma_1} \bar{W}_j \frac{\partial N_i}{\partial n} \, d\Gamma + \int_{\Gamma_2} \bar{\bar{W}}_j \, N_i \, d\Gamma$$

$$f_j = \int_{\Gamma_1} \bar{W}_j \, \bar{q} \, d\Gamma + \int \bar{\bar{W}}_j \, \bar{\phi} \, d\Gamma + \int_{\Gamma_1} \bar{W}_j \frac{\partial \varphi}{\partial n} \, d\Gamma - \int_{\Gamma_2} \bar{\bar{W}}_j \, \varphi \, d\Gamma \tag{20a}$$

(20b)

where $\varphi$ is any function satisfying the equation (9a) exactly and

$$\hat{\phi} = \sum N_i \, a_i + \varphi \tag{21}$$

For clarity we shall omit the non-homogeneous term in future derivations although it can readily be retained.

To obtain symmetric approximation forms is now somewhat more difficult and various alternatives are present. For instance if $\bar{W}$ and $\bar{\bar{W}}$ are chosen as

$$\bar{W}_j = \frac{\partial N_j}{\partial n}$$
$$\bar{\bar{W}}_j = \alpha N_j \qquad (22)$$

we have an alternative derivation of an approximation previously derived by the use of a least square, variational, approximation (7).

However an alternative form is possible and this is obtained by putting

$$\bar{W}_j = N_j$$
$$\bar{\bar{W}}_j = -\frac{\partial N_j}{\partial n} \qquad (23)$$

If we observe that for any two functions $N_i$ and $N_j$ which satisfy the Laplacian equation we can write, using Green's theorem, the following identity

$$\int_\Gamma \left(N_i \frac{\partial N_j}{\partial n} - \frac{\partial N_i}{\partial n} N_j\right) d\Gamma = \int_\Omega (N_i \nabla^2 N_j - N_j \nabla^2 N_i) d\Omega = 0$$

then the symmetry becomes evident. Inserting equation (23) into equation (20a) and adding half of the left-hand-side of above identity equation, we have

$$H_{ij} = \int_{\Gamma_1} N_i \frac{\partial N_i}{\partial n} d\Gamma = \int_{\Gamma_2} \frac{\partial N_j}{\partial n} N_i d\Gamma + \frac{1}{2}\int_{\Gamma_1+\Gamma_2} \left(N_i \frac{\partial N_j}{\partial n} - \frac{\partial N_i}{\partial n} N_j\right) d\Gamma =$$
$$= \int_{\Gamma_1} \left(\frac{1}{2} N_j \frac{\partial N_i}{\partial n} + \frac{1}{2} N_i \frac{\partial N_j}{\partial n}\right) d\Gamma - \qquad (24)$$
$$- \int_{\Gamma_2} \left(\frac{1}{2} N_j \frac{\partial N_i}{\partial n} + \frac{1}{2} N_i \frac{\partial N_j}{\partial n}\right) d\Gamma$$

This form has again been derived using an energy variational principle and has been used effectively in many boundary type solutions (7). We shall see later that this form leads more readily to the symmetric coupling of standard finite element and boundary solution procedures.*

## 5. SINGULAR FUNCTIONS AND INTEGRAL EQUATION FORMULATIONS

In the boundary solution methods just described one of the major difficulties is obviously that encountered in generating "complete" sets of trial functions $N_i$ which satisfy the governing equations. It is however relatively simple to obtain singular Green's type solutions for the full space which do satisfy all the boundary conditions in an infinite region or even with some simple conditions imposed at intermediate boundaries. If a distribution of such singularities with an intensity $\mu$ is placed on the problem boundary we can write for any point the function $\phi$ and its derivatives in the form of an integral equation. Thus for a homogeneous linear operator such as that of equation (16) we can write

$$\phi(s) = \int_\Gamma G(s,\Gamma)\mu \, d\Gamma \qquad (25)$$

where $G$ is a suitable Green's function and $\mu(\Gamma)$ is the intensity of the singularity distribution.

This represents a Fredholm integral equation of the first kind when the boundary conditions specify the values of $\phi$. By differentiation of the above expression Fredholm integral equations of the second kind arise when mixed boundary conditions are specified.

The solution can now be approached via a direct discretisation of the integral equation or by returning to a definition of shape functions defined in equation (16).

Thus if we write

$$\mu(\Gamma) = M_i a_i \qquad (26)$$

where $M_i(\Gamma)$ is an appropriate interpolation of intensity we can write the approximation in the form

$$\phi \approx \hat{\phi} = \int_\Gamma G(s,\Gamma) M_i \, d\Gamma \, a_i \qquad (27)$$

This automatically defines the shape function

---

*It is of interest to observe that the choice of weighting functions is limited to non-zero values. If for instance the trial functions $N_i$ include constant terms the weighting functions given by equation (23) will have some zero values. This will lead to difficulty of the determination of the constant parameters. The avoidance of the difficulty is discussed elsewhere in detail.

$$N_i = \int_\Gamma G(s,\Gamma) M_i \, d\Gamma \tag{28}$$

and all the general procedures previously developed are applicable.

We must note however that the definition of the normal derivatives may take a rather special form now. For instance if $G$ corresponds to source functions in the Laplacian problem we must write

$$\frac{\partial N_i}{\partial n} = \int_\Gamma \frac{\partial G}{\partial n} M_i \, d\Gamma + \frac{1}{2} M_i \tag{29}$$

where the last term is by no means self-evident but arises due to integration of the singularity.

It appears that the interpretation of the integral equation in terms of standard shape functions is inconvenient involving as it does a complicated integration. This difficulty is however not serious although a direct weighting of integral equations can be often achieved and apparently simpler results obtained.

We can thus write for instance the weighted form of the integral operator along the boundary as

$$\int_\Gamma W_j \left[ \int_\Gamma G(s,\Gamma) M_i \, d\Gamma \, a_i - \bar{\phi} \right] ds = 0 \tag{30}$$

This again leads to approximation of the form of equation (18), i.e.

$$\underset{\sim}{H}\,\underset{\sim}{a} = \underset{\sim}{f}$$

with

$$H_{ji} = \int_\Gamma W_j(s) \int_\Gamma G(s,\Gamma) M_i(\Gamma) \, d\Gamma \, ds$$
$$f_j = \int_\Gamma W_j \bar{\phi} \, d\Gamma \tag{31}$$

This form will be symmetric providing

$$G(s,\Gamma) = G(\Gamma,s) \tag{32}$$

and if the Green's function $G$ is symmetric i.e.

$$M_i = W_j \tag{33}$$

This approximation is not identical with that of equations (27,28) and we shall later see is not suitable for use in the coupling procedures.



It can be shown that the integral equation (25) is incomplete (and does not possess a finite solution) for all specified boundary conditions. For such completeness it is desirable to supplement the source distribution $\mu$ by a distribution of doublets $\lambda$ and now we can write (for points on a smooth boundary)

$$\pi\phi(s) = \int_\Gamma G(s,\Gamma) \mu \, d\Gamma - \int_\Gamma \frac{\partial G(s,\Gamma)}{\partial n} \lambda \, d\Gamma \tag{34}$$

After some manipulation we can identify

$$\mu = \frac{\partial \phi}{\partial n} \qquad \lambda = \phi \tag{35}$$

In this form the direct identification of shape functions does not appear simple but the weighting process once again can be applied to the integral form. Thus for a Dirichlet problem where

$$\phi - \bar{\phi} = 0$$

we have (36)

$$\int_\Gamma N_j(s) \left[ \pi\phi(s) - \int_\Gamma G(s,\Gamma) \mu(\Gamma) \, d\Gamma + \int \frac{\partial G(s,\Gamma)}{\partial n} N_i(\Gamma) \, d\Gamma \, \phi_i \right] ds$$

This again will result in equations similar to Eq. 31 which can be made symmetric

## 6. COMBINED "STANDARD" FINITE ELEMENT AND "BOUNDARY" SOLUTIONS

In the "standard" finite element process simple, locally based polynomial functions are normally used and their approximation can be easily written for non-homogeneous and non-linear situations. A limitation, however, arises when infinite domains are encountered and in general a large number of unknowns is involved.

In the "boundary" solution technique on the other hand a smaller number of unknowns is generally involved and infinite domains are dealt with simply. However these have to be generally linear and homogeneous.

Clearly the simultaneous use of both sub-classes is desirable and in this section we shall investigate such a coupling shown diagrammatically in Figure 2. To simplify the presentation we shall limit ourselves to the illustrative problem of equation (9) (with $K = 1$ in boundary domain $\Omega^{(e)}$). In the notation we shall use the superscript $\sim$ to denote quantities of the finite element region while those of the boundary domain are written without a superscript.

Thus for the finite element method domain we can write

$$\tilde{\underset{\sim}{H}}\,\tilde{\underset{\sim}{\phi}} = \tilde{\underset{\sim}{f}} \tag{37}$$

where $\tilde{\phi}$ stands now for the nodal values of $\phi$. A symmetric (Galerkin) formulation is generally used and we can write (viz. Eq. 13)

$$\tilde{H}_{ji} = \int_{\Omega^e} \underset{\sim}{\nabla}^T \tilde{N}_j \, k \, \underset{\sim}{\nabla} N_i \, d\Omega$$

$$\tilde{f}_j = \tilde{f}_{j0} - \int_I N_j \bar{q} \, dI \tag{38}$$

where

$$\bar{q} = -k \frac{\partial \phi}{\partial n} \quad ; \; k = 1$$

are fluxes specified on the interface and supplied by the solution of the boundary domain. We can therefore write

$$\frac{\partial \phi}{\partial n} = \frac{\partial N_i}{\partial n} a_i \tag{39}$$

**

We can thus write

$$\tilde{\underset{\sim}{H}}\,\tilde{\underset{\sim}{\phi}} + \underset{\sim}{A}\,\underset{\sim}{a} = \tilde{\underset{\sim}{f}}_0 \tag{40}$$

where

$$A_{ji} = \int_I \tilde{N}_j \frac{\partial N_i}{\partial n} \, dI$$

If we now turn to the boundary domain we have, following equations (19-21)

$$\underset{\sim}{H}\,\underset{\sim}{a} = \underset{\sim}{f} \tag{41}$$

where again considering only prescribed $\phi$ condition on the interface we can write

$$\phi = \bar{\phi} = \tilde{N}_i \tilde{\phi}_i \tag{42}$$

**Note that in above we have implied that all prescribed values of $\tilde{\phi}$ are automatically situated in the finite element domain and that prescribed fluxes on its boundary are included in $\tilde{f}_0$.

$$H_{ji} = \int_I \bar{N}_j N_i \, dI \tag{43a}$$

and

$$f_j = f_{j0} + \int_I \bar{W}_j \tilde{N}_i \, dI \, \tilde{\phi}_i \tag{43b}$$

Thus we have in place of equation (41)

$$\underset{\sim}{H}\,\underset{\sim}{a} + \underset{\sim}{B}\,\tilde{\underset{\sim}{\phi}} = \underset{\sim}{f}_0 \tag{44}$$

where

$$B_{ji} = -\int_I \bar{W}_j \tilde{N}_i \, dI$$

Equations (40) and (44) for the whole system can be written now as

$$\begin{bmatrix} \tilde{H} & , & A \\ B & , & H \end{bmatrix} \begin{Bmatrix} \tilde{\phi} \\ a \end{Bmatrix} = \begin{Bmatrix} \tilde{f}_0 \\ f_0 \end{Bmatrix}$$

and in principle can be solved. We note in the above that

(a) the boundary region can be treated just as another element

and

(b) that the matrices $A$ and $B$ do not overlap for interior values of $\tilde{\phi}$ which give zero contributions at the interface.

As the standard finite element formulation has made use of symmetry it remains to be seen whether the whole system once again can be made symmetric. In equations (22) and (23) we have given such possibilities for the boundary domain but we see now that only the second form of weighting functions will result in a symmetry of the combined system. This now gives

$$B_{ji} = \int_I \frac{\partial N_j}{\partial n} \tilde{N}_i \, dI \equiv A_{ij} \tag{45}$$

and full symmetry is observed.

Similar results are clearly available if the solution of the boundary regions stems from the singularity distribution or its integral equation form. If the singularity distributions are presented in terms of final shape functions such as given in equation (28) then obviously all the above statements are true and symmetrising is done in precisely the same manner as above.

On the other hand if the approximation process starts from a direct discretisation of the integral equation in the manner given in equations (30-31) then some difficulties appear to arise. The reader can verify now that the matrix has the form

$$B_{ji} = \int_\Gamma N_j \tilde{N}_i \, d\Gamma \tag{46}$$

and similarly that

$$A_{ji} = \int_\Gamma \tilde{N}_j \left( \int_\Gamma \frac{\partial G}{\partial n} M_i \, d\Gamma + \tfrac{1}{2} M_i \right) d\Gamma \tag{47}$$

To obtain symmetric equations we must now take

$$N_j = \int_\Gamma G M_i \, d\Gamma$$

as a weighting function. It will be seen that the result is of a form identical to that used in the more general preceding form.

For the integral equation of the form (34) a symmetric form is even more difficult to produce and we shall not discuss the details of the procedure here.

## GENERAL REMARKS ON THE COUPLING PROCESS

In much of the development of the boundary solution process and in particular in the application of singular solutions, collocation methods have been used to avoid the difficulty of double integration. This inevitably leads to non-symmetric equation forms as was shown previously and considerable computational difficulties arise which have to be balanced against the cost of symmetry and the possibilities of combining both methods in one "standard" finite element package. Much work has yet to be done on overcoming some of the difficulties of such coupling and indeed in streamlining the boundary integral equation forms and some of the problems are discussed elsewhere (8).

In the practical application of mathematical problems it is most likely that the boundary solution methods will be confined to the exterior domains and more standard finite element processes used where non-linearities are encountered. This is an opinion based on some experience although the possibility of using direct boundary solutions in non-linear domains has been actively investigated and in some situations appears economic.

One point of some importance is the fact that the use of boundary type elements couples all the parameter values of the finite element solution along the interface, thus resulting in large bandwidths for final equations, Figure 3a. If the boundary elements are confined to exterior regions two possible ways of alleviating this difficulty arise.

(a) the number of parameters $\underset{\sim}{a}$ and hence of the interpolating singularity values is kept low

or

(b) the exterior region is subdivided into a series of "radial" strips thus coupling a narrower band of finite element parameters.

This introduces the problem of interfaces between such radial strips which however can be dealt with by standard process.

The last possibility can be implemented by the use of "infinite" elements (5) where the trial functions are locally based and only approximate the solution of the actual differential equations. Much current work has shown the efficiency of such approximations but many possibilities yet remain to be explored.

## CONCLUDING REMARKS AND RELEVANCE TO MAGNETO-STATIC PROBLEMS

Various methods of approach have been applied to the formulation of magneto-static problems which arise from the following general conditions.

$$\text{(a)} \quad div \underset{\sim}{B} \equiv \underset{\sim}{\nabla}^T \underset{\sim}{B} = 0$$

$$\text{(b)} \quad curl \underset{\sim}{H} \equiv \underset{\sim}{\nabla}^T \times \underset{\sim}{H} = \underset{\sim}{J} \tag{48}$$

$$\text{(c)} \quad \underset{\sim}{B} = \mu(|H|) \cdot \underset{\sim}{H} \qquad |H| = \sqrt{H_x^2 + H_y^2 + H_z^2}$$

A very thorough survey of the possibilities offered by various formulations is given by Simkin and Trowbridge (9). In that paper various integral equations or differential relationships are presented. With the general definition of the finite element process it is clear that the previous procedures could be applied to the numerical solution of any such discretisation.

The essential three types of formulation are given by

(1) the use of magnetisation vector

$$\underset{\sim}{M} = (\mu - 1) \underset{\sim}{H} \tag{49}$$

as the basic variable. Noting that $\underset{\sim}{M} \equiv 0$ in the domain exterior to magnetic materials the problem domain is small. This involves however integral equations which have to be defined over the domain and is the basis of the GFUN program. Here many alternatives of weighting are presented and the one used in the program has advantages of simplicity although it involves non-symmetric forms. Symmetric formulation is however possible and could well be explored.

(2) The use of vector potential $\underset{\sim}{A}$ defining

$$\underset{\sim}{B} = \text{curl}\,\underset{\sim}{A} = \underset{\sim}{\nabla}^{r} \times \underset{\sim}{B} \tag{50}$$

this automatically eliminates equation (48a) as

$$\text{div curl}\,\underset{\sim}{A} \equiv 0 \tag{51}$$

and results in a final equation in a single variable $\underset{\sim}{A}$ which is

$$\underset{\sim}{\nabla}^{r} \times \frac{1}{\mu} \underset{\sim}{\nabla}^{r} \times \underset{\sim}{A} = \underset{\sim}{J} \tag{52}$$

This general form needs a subsidiary condition and introduces many difficulties in formulation for a full three-dimensional problem. However in two dimensional analysis the use of vector potential with a single component has now become very widespread and falls precisely under the category of the illustrative example discussed throughout this paper.

(3) The final possibility is the use of scalar potentials to define the field

$$\underset{\sim}{H} = \underset{\sim}{\bar{H}} + \underset{\sim}{\nabla}\phi \tag{53}$$

Here an auxiliary function $\underset{\sim}{\bar{H}}$ is introduced in sub-domains in which $J \neq 0$ so that

$$\text{curl}\,\underset{\sim}{\bar{H}} = \underset{\sim}{J} \tag{54}$$

Now once again we find that the problem has been defined by standard Poisson equation which however is now applicable in three-dimensional as well as two-dimensional domains. As equation (48b) is identically satisfied the governing equation is now simply of the form resulting from equation (48a)

$$\underset{\sim}{\nabla}^{r} \cdot \underset{\sim}{\nabla}\phi + \underset{\sim}{\nabla}^{r} \cdot \underset{\sim}{\bar{H}} = 0 \tag{55}$$

Use of the finite elements in a particular form of this solution has been discussed and applied by Zienkiewicz et al (19) but led, as shown later, to a numerical inaccuracy in magnetic domains. A modification of the process using a discontinuous defined function $\bar{H}$ has recently been introduced by Simkin and Trowbridge (9) and leads to an excellent numerical accuracy.

In this formulation we take where is equal to

$$\bar{H} = H_s \qquad H_s = \frac{1}{4\pi} \int_{\Omega_J} \frac{\underset{\sim}{J}(\underset{\sim}{r} - \underset{\sim}{r}')}{|\underset{\sim}{r} - \underset{\sim}{r}'|^3}\, d\Omega_J \tag{56}$$

for the part of the whole domain which includes the current carrying elements and also extends to infinity. In the remaining portion taken over the magnetising region we simply impose

$$\bar{H} = 0 \tag{57}$$

The discontinuity of $\bar{H}$ is easily accounted for on the interface in the general forms of equations derived in this paper and we shall not discuss this in detail.

It appears that the last form of the procedures utilising the scalar potential approach is the most powerful and can be made very economical for two and three-dimensional solution of all magneto-static problems.

Although the discussions of this paper have taken as specific example the Poisson equation in the real domain it is simple to extend the generality to other equations pertaining to magneto-statics and many papers at this symposium will show one or other forms of such approximations.

## REFERENCES


1. Strang, G and Fix, G. J., An analysis of the Finite Element Method, Prentice-Hall, 1973.

2. Mitchell, A. R. and Wait, R. The Finite Element Method in Partial Differential Equations. J. Wiley & Sons, 1977.

3. Zienkiewicz, O. C. The Finite Element Method, 3rd ed. McGraw-Hill 1977.

4. Zienkiewicz, O. C., Kelly, D. W., Bettess, P. The finite element method for determining fluid loadings on right structures' Ch.4 of Numerical Methods in Offshore Engineering, ed. O. C. Zienkiewicz, R. Lewis and K. G. Stagg, J. Wiley & Son, 1977.

5. Bettess, P. Infinite elements, Int. J. Num. Meth. Eng., 11, 53-64, 1977.

6. Trefftz, E. Gegenstück zom Ritz'schen Verfahren, Proc. Sec. Int. Congress Applied Mechanics, Zurich, 1926.

7. Zienkiewicz, O. C., Kelly, D. W. and Bettess, P. The coupling of the finite element method and boundary solution procedures, Int. J. Num. Meth. Eng., 11, 355-76, 1977. (See also Proc. World Congress on finite elements in structural mechanics, 1975).

8. Zienkiewicz, O. C., Kelly, D. W. and Bettess, P. Marriage a la mode - Finite elements and boundary integrals, in Proc. Conf. Innovative Numerical Analysis in Engineering Science, CETIM, Paris 1977.

9. Simkin, J. and Trowbridge, C. W. Which Potential? A comparison of the various scalar and vector potentials for the numerical solution of the non-linear Poisson problem. Rutherford Laboratory 1978. RL-78-009/B.

10. Zienkiewicz, O. C., Lyness, J. and Owen, D. R. J. Three dimensional magnetic field determination using a scalar potential - a finite element solution. IEEE (Magnetics Trans.) p.1649-56, MAG-13, 1977.

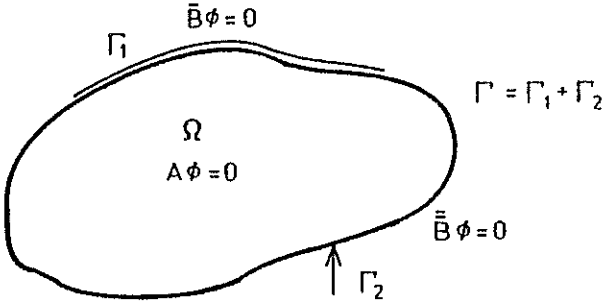


*FIGURE 1 The problem 'domain' $\Omega$ and its' boundaries $\Gamma$*

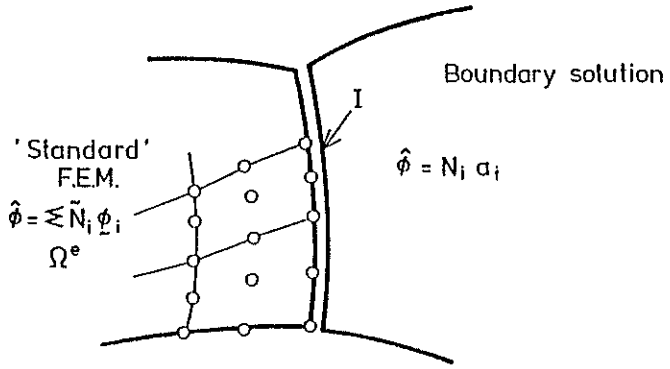


*FIGURE 2 Coupling of 'standard' F.E.M. with boundary solution.*

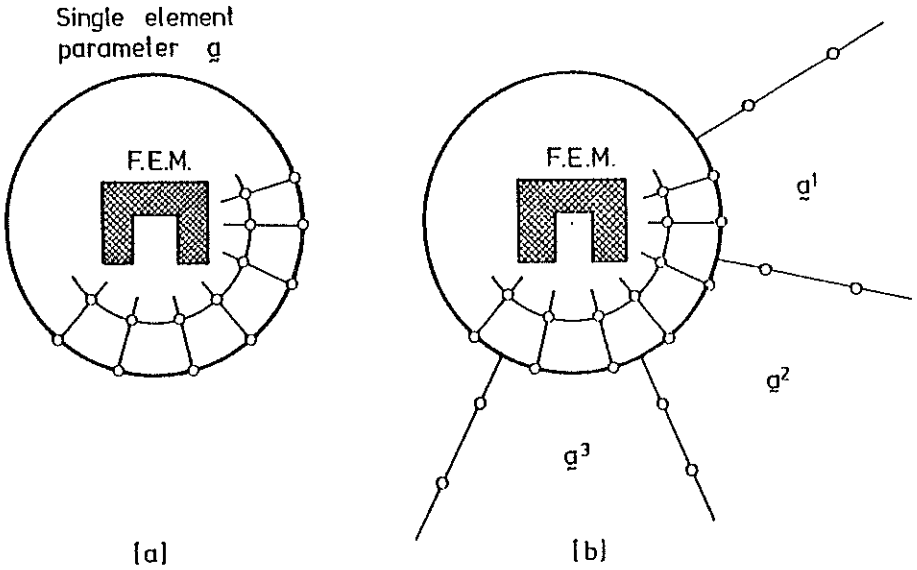


*FIGURE 3 Exterior boundary elements*
*a. Single exterior element*
*b. Strip infinite element*

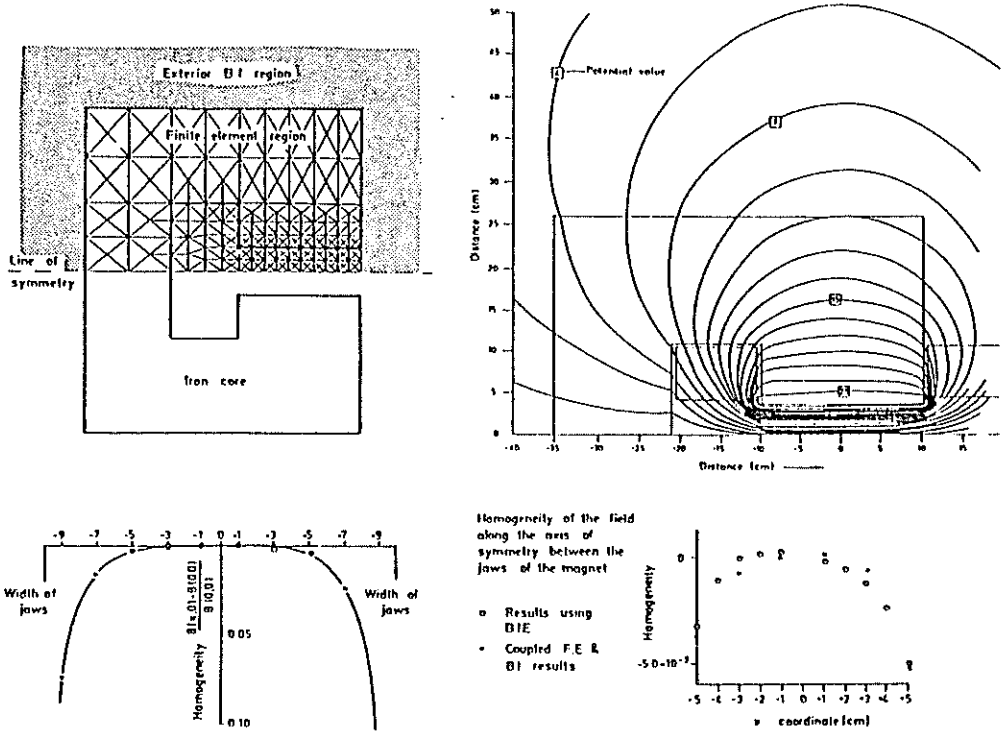


*FIGURE 4 A two-dimensional coupled solution*

# THE SOLUTION OF 3D MAGNETOSTATIC PROBLEMS USING SCALAR POTENTIALS

A G Armstrong, C J Collie, J Simkin, C W Trowbridge

Rutherford Laboratory, Chilton, OXON, UK.

## ABSTRACT

The three dimensional magnetostatic problem is formulated using a combination of two scalar potentials. The potential associated with the total field is used for points interior to current free iron domains to ensure good numerical stability. In exterior regions the reduced potential associated with the induced field is used. Results from computer codes using both differential and integral operators are presented, and compared with measured values. Significant improvements over existing codes are anticipated.

## 1. INTRODUCTION

In two dimensions magnetostatic fields can be computed to a very high accuracy even when the geometry of the problem is complicated.[1,2,5,9] However in three dimensions computer programs are expensive to run and can only give accuracies of the order of 1% in most cases.[8,11,12] It is convenient to compute the fields from current sources analytically or by quadrature, thus reducing the complexity of the mesh needed for differential methods and allowing the possibility of using integral methods. The remaining part of the field is produced by induced sources and this can either be solved for directly by computing the magnetisation vector or by computing the associated scalar potential. The former approach leads to an integral equation formulation [3,4,5] and the latter to both differential [11,12] and integral variants.[10] Of special interest for linear problems in this context is the use of boundary integral procedures also based on the reduced scalar potential.[7,14] The advantage of a scalar potential for three dimensional problems is of course that there is only one unknown quantity for each mesh point. However it has been shown that the use of this reduced scalar potential leads to inaccurate fields inside iron regions.[16] To overcome this difficulty it was proposed to use a formulation based on the total potential in regions when this is unique (ie current free) and the reduced potential elsewhere. This procedure has been tested for a range of two dimensional non-linear problems using a differential finite element formulation.[16] The choice of whether to adopt integral or differential procedures is not easy and there are good arguments either way depending upon context. In this paper the results from both differential and integral operator formulations are presented using the combined total and reduced potential procedure extended to three dimensional linear and non-linear problems.

## 2. FIELD EQUATIONS AND CHOICE OF POTENTIAL

In magnetostatics the current density $\underline{J}$ is known, and occupies a part of the problem space $\Omega_J$. The magnetisation $\underline{M}$ whether induced by the current or supplied by permanent magnetic material occupies a region $\Omega_I$; thus if the total field $\underline{H}$ is expressed as the sum the field of the sources $\underline{H}_S$ and the induced magnetisation $\underline{H}_M$

$$\underline{H} = \underline{H}_M + \underline{H}_S \tag{2.1}$$

then $\underline{H}_S$ is known from $\underline{J}$

$$\underline{H}_S = \frac{1}{4\pi} \int_{\Omega_J} \underline{J} \times \nabla\left(\frac{1}{R}\right) d\Omega \tag{2.2}$$

or $\nabla \times \underline{H}_S = \underline{J}$

which implies $\nabla \times \underline{H}_M = 0$

hence $\underline{H}_M$ can be expressed as the gradient of a scalar $\phi$.

Thus $$\underline{H}_M = -\nabla\phi \tag{2.3}$$

with $$\phi = \frac{1}{4\pi} \int_{\Omega_I} \underline{M} \cdot \nabla\left(\frac{1}{R}\right) d\Omega$$

and $R = |\underline{r}' - \underline{r}|$ is the distance from the source point $\underline{r}'$ to the field point $\underline{r}$ (see Figure 1).

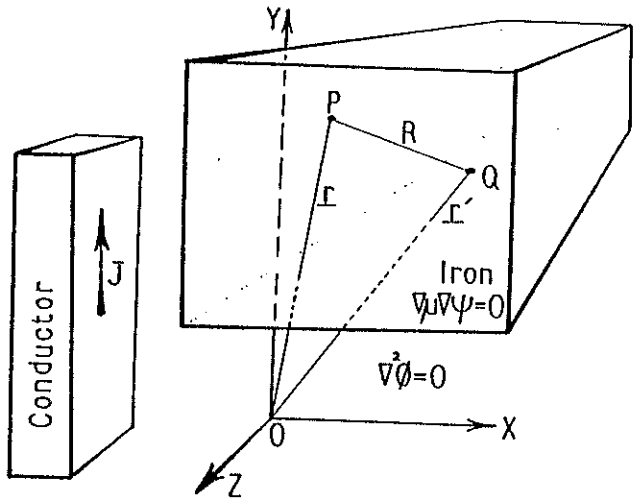


FIG. 1 POTENTIAL REGIONS AND BASIC GEOMETRY

The flux density $\underline{B}$, $\underline{H}$ and $\underline{M}$ are further related by the constitutive equations for magnetic materials:

$$\underline{B} = \mu(|H|)\ \underline{H} = \mu_o(\underline{M} + \underline{H}) \qquad (2.4)$$

$$\underline{M} = \chi(|H|)\ \underline{H}$$

with $\nabla\cdot\ \underline{B} = 0$ (2.5)

and $\mu_o$ is the permeability of free space.

From equations (2.4), (2.3) and (2.1) $\underline{B} = \mu(\underline{H}_S - \nabla\phi)$. If $\underline{H}_S$ is large compared with $\underline{H}$, this is clearly[16] ill conditioned if the variable solved for is $\phi$. It is then preferable to solve for the difference quantity $\underline{H}$ directly. Moreover for current free regions this can be done by solving for a total scalar potential $\psi$

$$\underline{H} = -\nabla\psi \text{ (valid when } \nabla \times \underline{H} = 0). \qquad (2.6)$$

This leads (by equation (2.5)) to the pair of equations:

$$\nabla\cdot(-\mu\nabla\psi) = 0 \quad \text{(when valid)} \qquad (2.7)$$

$$\nabla\cdot(-\mu\nabla\phi + \mu\underline{H}_S) = 0 \quad \text{(elsewhere)} \qquad (2.8)$$

which are non linear PDE's of the Laplace and Poisson type respectively. In addition to the external boundary conditions: $\phi \to 0$ at infinity for example, there are interface conditions between a $\psi$ region (subscript 1) and a $\phi$ region (subscript 2).

$$-\mu_1\ \partial\psi/\partial n = \mu_2(-\partial\phi/\partial n + \underline{H}_{Sn}) \qquad (2.9)$$

$$-\partial\psi/\partial t = -\partial\phi/\partial t + \underline{H}_{St} \qquad (2.10)$$

where n and t denote the normal and tangential components respectively.

Equation (2.10) can be integrated immediately to give the contribution $\psi_S$ to the total potential

$$\psi_S = \psi - \phi = -\int \underline{H}_{St}\ dt \qquad (2.11)$$

It is shown in the next section that knowledge of $\underline{H}_S$ on the interface is sufficient to determine the problem, so that equation (2.11) is more useful than equation (2.10). The arbitary constant in equation (2.11) is removed by equating $\psi$ and $\phi$ at some convenient interface point.

To ensure that the total scalar potential in multiply connected regions be single valued, suitable cuts are made in the iron.



## 3. DIFFERENTIAL FORMULATION

The PDE's (2.7) - (2.8) are to be solved simultaneously by dividing the space into finite elements and applying a weighted residual technique.[15] For the case of region 1 being non-linear iron and region 2 free space with conductors, the residual equations are respectively:

$$R_1 = \int_{\Omega_1} W\ \nabla\cdot(-\mu\nabla\psi)\ d\Omega$$

$$R_2 = \int_{\Omega_2} W\ \nabla\cdot(-\nabla\phi)\ d\Omega \qquad (\text{since } \nabla\cdot\underline{H}_S = 0)$$

for any suitably chosen weighting function W. However, to allow the introduction of local basis functions for $\phi,\psi$ without the restriction of second order continuity across elements, these are transformed by Green's theorem to:

$$R_1 = \int_{\Omega_1} \mu\nabla W\cdot\nabla\psi d\Omega - \int_{S_1} \mu W\nabla\psi\cdot d\underline{S} \qquad (3.1)$$

$$R_2 = \int_{\Omega_2} \nabla W\cdot\nabla\phi d\Omega - \int_{S_2} W\nabla\phi\cdot d\underline{S}. \qquad (3.2)$$

This requires W to be continuous across the interface and differentiable within $\Omega_1$ and $\Omega_2$.

Setting $R_1 + R_2 = 0$ gives:

$$\int_{\Omega_1} \mu\nabla W\cdot\nabla\psi d\Omega + \int_{\Omega_2} \nabla W\cdot\nabla\phi d\Omega = \int_{S_1} W(\mu\frac{\partial\psi}{\partial n} - \frac{\partial\phi}{\partial n})\ dS$$

$$= -\int_{S_1} W\underline{H}_{Sn}\ dS \qquad (3.3)$$

where the last form follows from the interface condition (2.9), and only the common surface between iron and space contributes because $\phi \to 0$ at infinity.

A set of basis functions N(x,y,z) is chosen so that in each of the elements

$$U = N_1U_1 + N_2U_2 + N_3U_3 \ \ldots\ldots \qquad (3.4)$$

where U is $\psi$ or $\phi$ according to which region contains the element; $U_i$ is the value of U at the element mode i, and $N_i$ is 1 at node i and 0 at the other nodes of the elements. The Galerkin[15] procedure is to choose a weight function W for each node i which equals the appropriate $N_i$ for each element containing node i and is zero elsewhere. Equation (3.3) then yields one equation for each node i:

$$\sum_{\text{elements containing node } i} \Big\{ \sum_{\text{nodes } j \text{ in such an element}} \Big[ \psi_j \int \mu \nabla N_i \cdot \nabla N_j \, d\Omega + \phi_j \int \nabla N_i \cdot \nabla N_j \, d\Omega \Big] - \int_{S_i} N_i \, \underline{H}_{Sn} \, dS \Big\} = 0 \qquad (3.5)$$

Since a node i in the interface requires two unknowns, $\psi_i$ $\phi_i$, the interface condition (2.11) is used to eliminate $\phi$ or $\psi$ for such nodes. The surface integral in equation (3.5) is zero for i not in the interface, even if elements containing i meet it, since $N_i$ is zero on an element facet not containing i. For the volume terms the equations will only have non-zero coefficients for both $\psi$ and $\phi$ if i is in the interface.

Equation (3.5) thus produces a set of n linear equations for the $U_i$ of the form:

$$K_{ij} \, U_j = Q_i \qquad (3.6)$$

in which $K_{ij}$ is a banded symmetric matrix with elements which are sums of terms like:

$$k_{ij} = \int_{\text{element}} \mu \, \nabla N_i \cdot \nabla N_j \, d\Omega \qquad (3.7)$$

and the $Q_i$ are mostly zero, except for terms of the forms:

$$\sum_{\text{facets containing } i} \int N_i \underline{H}_{Sn} \, dS \quad \text{and} \quad k_{ij} \int_0^{t_j} \underline{H}_{St} \, dt \qquad (3.8)$$

for i, j in the interface. The $k_{ij}$ are generally obtained by quadrature but for certain elements they are simple analytic forms.[15]

## 4. INTEGRAL FORMULATION

When the iron is a current free region an integral equation can be set up in the total potential $\psi$. From equation (2.11):

$$\psi = \phi + \psi_s = \phi - \int \underline{H}_{St} \, dt \qquad (4.1)$$

in which $\psi_s$ is readily calculated from the prescribed conductors.

The reduced potential $\phi$ is now eliminated from equation (4.1) by equation (2.3) together with equations (2.4) and (2.6) to obtain

$$\psi(\underline{r}) = -\frac{1}{4\pi} \int_{\Omega_I} \chi(\underline{r}') \nabla\psi(\underline{r}') \cdot \nabla\left(\frac{1}{R}\right) d\Omega + \psi_S(\underline{r}) \qquad (4.2)$$

which is the required integral equation for $\psi$. It has of course no boundary conditions, and so can be solved by discretising only the iron. Once solved, the field $\underline{H}$ can be readily obtained anywhere in space from:

$$\underline{H} = -\nabla\phi + \underline{H}_S \qquad (4.3)$$

since the equation (2.3) for the induced field is valid throughout space. The solution of (4.2) is thus in effect a complete solution of the problem.

Before discretising, it is worthwhile to transform equation (4.2) by Green's theorem and by the identity:

$$-\frac{1}{4\pi} \int_\Omega \nabla^2\left(\frac{1}{R}\right) d\Omega = \begin{cases} 1 \text{ for } \underline{r} \text{ inside} \\ 0 \text{ outside} \end{cases} \qquad (4.4)$$

$$\mu\psi(\underline{r}) = -\frac{\mu_o}{4\pi} \int_{S_I} \chi(\underline{r}') \, \psi(\underline{r}') \nabla\left(\frac{1}{R}\right) \cdot dS + \frac{\mu_o}{4\pi} \int_{\Omega_I} \psi(\underline{r}') \nabla\chi(\underline{r}') \cdot \nabla\left(\frac{1}{R}\right) d\Omega + \mu_o \, \psi_S(\underline{r}) \qquad (4.5)$$

To solve equation (4.5) the iron is divided into elements. For linear problems the volume term vanishes. Even for non-linear problems a base function may be chosen for $\chi$ which enable the volume term to be transformed into integrals over the internal surfaces of the elements, so that only two-dimensional integrals over element surfaces are required. The plane triangular facet is chosen as a standard element.

Base functions for $\psi$ are chosen to be either linear or quadratic and are expressed in terms of area coordinates $L_1$, $L_2$, $L_3$ according to standard finite element practice[16].

First order (linear) elements:

$$\psi = L_1\psi_1 + L_2\psi_2 + L_3\psi_3 \qquad (4.6a)$$

Second order (quadratic) elements:

$$\psi = L_1(2L_1 - 1)\psi_1 + L_2(2L_2 - 1)\psi_2 + L_3(2L_3 - 1)\psi_3 + 4L_2L_3\psi_4 + 4L_3L_1\psi_5 + 4L_1L_2\psi_6 \qquad (4.6b)$$

where nodes 1 to 3 refer to vertices

and nodes 4 to 6 refer to mid-side points.

Both schemes of (4.6) have the property that the base functions are 1 at the appropriate node and 0 at the other nodes, as in the Galerkin scheme of equation (3.4). Either may be expressed formally as:

$$\psi = N_i\psi_i \text{ (summation convention applies)} \qquad (4.7)$$

Choosing the field point $\underline{r}$ in equation (4.5) to be each node in turn yields:

$$\mu\psi_i = K_{ij}\,\psi_j + \mu_o\,\psi_{Si} \qquad (4.8)$$

with

$$K_{ij} = \Sigma\ \frac{-\chi}{4\pi}\,\mu_o \int N_j\ \nabla\left(\frac{1}{R}\right)\cdot\, dS \qquad (4.9)$$

facets containing j

This leads to a set of equations with one equation for each $\psi_i$. The matrix $K_{ij}$ is dense and unsymmetric; however its components can be evaluated analytically using only elementary functions by the technique of reference (7).

Some comment is necessary on the singularity which occurs in the integrand of (4.9) when $R_i = 0$, that is, in those facets which contain the node i. To show that this does not invalidate the procedure consider the form of the base functions $N_j$: These are linear or quadratic functions of the coordinates, so choosing the coordinate origin near node i:

$$K_{ij} = \Sigma\ \frac{\chi\mu}{4\pi}\,\mu_o \int_{Lm\ \underline{r}\to\underline{r}_i} \nabla\left(\frac{1}{R}\right)(\delta_{ij} + b_1\,x + b_2 y\ \ldots)\ dS \qquad (4.10)$$

where the constant term is $\delta_{ij}$ since $N_j$ goes to 0,1 at the nodes; and $b_1$, $b_2$ are some constants. All terms in first or higher orders in the Cartesian coordinates x,y go to zero as $\underline{r}$ approaches $\underline{r}_i$. For the constant term however:

$$\int_{\text{facet}} \nabla\left(\frac{1}{R}\right)\cdot\, d\underline{S} = \int (\underline{r}'-\underline{r})R^{-3}\ d\underline{S} = \alpha \qquad (4.11)$$

where $\alpha$ is the solid angle subtended by the facet; while this is indeterminate for a single facet as the field point approaches a corner, the solid angle subtended by all the facets meeting at node i is calculated as $4\pi$ -(solid angle subtended by all other facets). $K_{ij}$ can therefore be set up, but the algorithm has to make special provision for the solid angle part of the self term.

In evaluating the fields from equation (4.3) after completing the $\psi$ solution corners and edges must be avoided since the field expression is singular there. Indeed to obtain sensible values of the fields at these locations would require the use of curved facets with smooth joins between them.

The extension of these ideas to non-linear problems presents no major difficulties. In addition to the iron domain surface discretisation there has to be a volume discretisation. In the present work it was decided to use a volume mesh of tetrahedra within which the permeability is constant. This approximation



offers an immediate test of the method since in effect the volume is replaced by a set of internal triangular facets over which the above equation (4.8) can be applied. A simple iteration scheme to improve the solution was employed which was found to converge in a few cycles. In order to update the permeability from the B-H curve the fields in the elements were obtained from volume shape functions using the nodal values of potential.

## 5. RESULTS

### Boundary Integral (constant permeability)

#### Data Generation

The program requires the surface of each unique iron region of the problem to be covered by a continuous triangular mesh, excluding faces which lie on planes of symmetry. The mesh triangles are called facets. The scalar potential is calculated at the mesh nodes for a first-order variation, and in addition at the mid-side positions for a second-order variation.

#### Hollow Sphere in a constant external field

This example serves as an analytic check on the computer program. Because the sphere has three planes of symmetry it can be represented by an octant. An example of one of the triangular meshes used is shown in Figure 2. Results for the field inside the cavity using both first and second

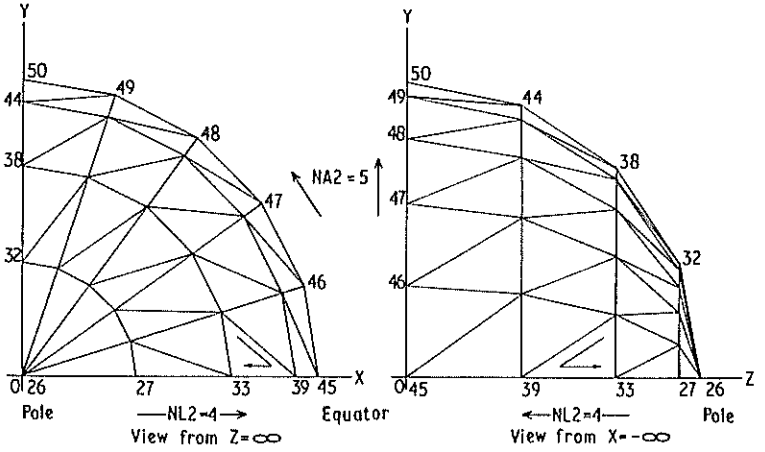


TRIANGULAR MESH ON OUTER SURFACE OF A SPHERE (with node numbers)

FIG. 2

order elements are shown in Figure 3, for a range of discretisations. The quantity actually computed is of the order 1-0.005 T = 0.995 T hence the accuracy obtained using second order elements is better than 0.1% . Good predictions were also obtained at all other points.

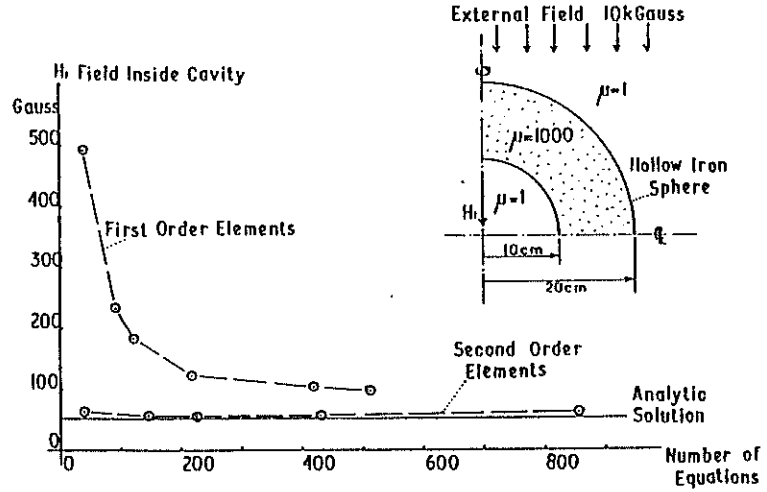


FIG. 3 CENTRAL FIELD IN A HOLLOW SPHERE

Bending magnet BM105

This magnet was chosen as a test case since comprehensive measurments in the end region were readily available[17].

This magnet is of window-frame construction (Figure 4) with bedstead coils which have 96 turns and give a central field of 0.79 Tesla at 1000 Amps in a gap of 6 inches. Only slight saturation effects are found at this current and the m.m.f lost in the yoke is about 0.1%. The coils are protected by iron guard plates which have magnetic connections to the yoke and which thereby constitute a single iron region.

Because it has three planes of symmetry the yoke of BM105 is representable by an octant (as in Figure 4), the developed surface of which is shown in Figure 5. This figure also shows a mesh of 392 facets which was sometimes used; it gives a problem of 204 unknowns (first-order) and 801 unknowns (second-order), since most nodes are shared by several facets.

The vertical component of magnetic field $B_y$, was calculated at several of the positions on the Y=0 plane where it has been measured.

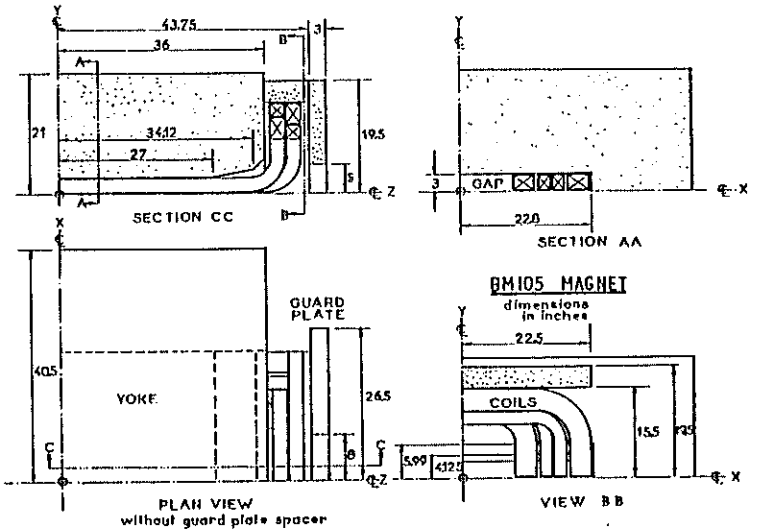


FIG. 4 OCTANT OF BENDING MAGNET BM105

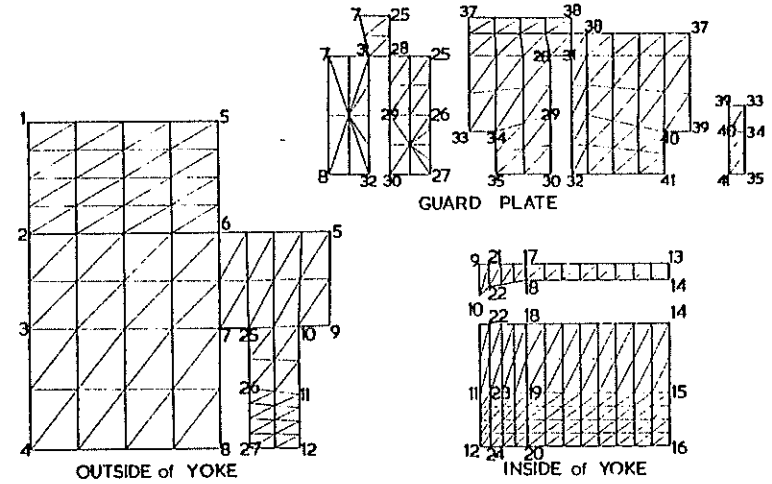


BM 105 MAGNET TRIANGULATED IRON SURFACE (392 FACETS)

FIG. 5

The distribution along the line (X=0,Y=0) is shown in the upper part of Figure 6; to make the results easier to assess, the differences between the calculations and the measurement are shown in the lower part. There was a significant reduction in the differences in changing from first to second order, but very little change in the second-order results when many extra facets were arranged at the end of the pole face and end face of the yoke. The largest differences occured at Z=36", where the yoke ends and the field changes by about 10% per inch (=3.2 $Tm^{-1}$): they were 0.4% (second-order) and 1.8% (first-order). The calculations assumed a constant permeability of 3000, but there was no significant change when this was reduced to 1000. Small changes in the ends of the coils were unimportant and it seemed that a third-order variation would be needed to make further improvements.

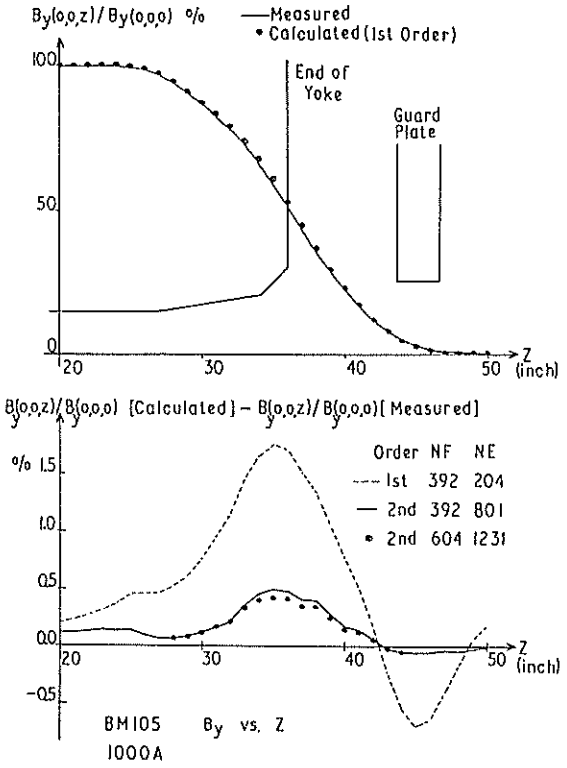


FIG. 6 BM105 COMPARISON OF MEASUREMENT WITH COMPUTATION ON CENTRE LINE

The transverse field distribution near the end of the yoke is shown in Figure 7; the measured results are on the left, the others are calculated. Positions Z=30" and 35" are under the pole, 38" and 42" between the yoke and the guard plate, and 46" almost out of the outside of the guard plate. The biggest discrepancies occur at Z=38" and 46", amounting to about 5mT at X=6.5" with second-order variation. The first-order model is obviously too coarse.

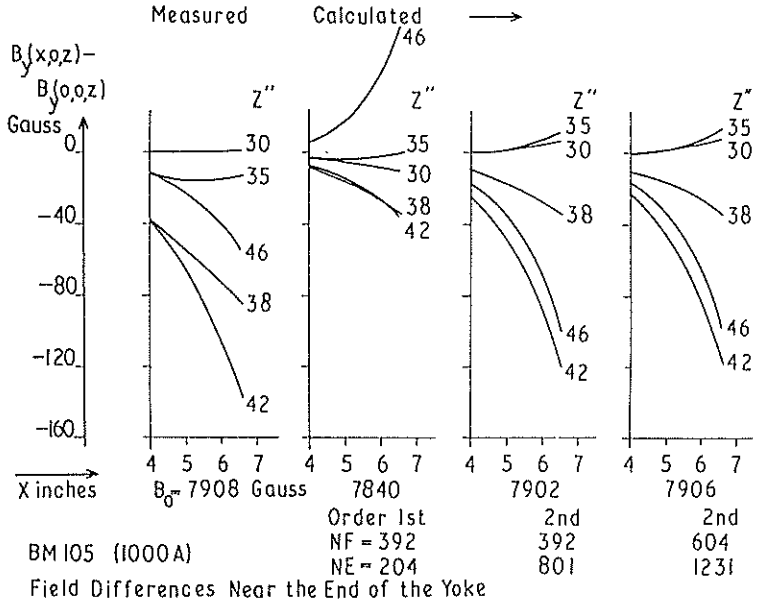


FIG. 7

## Boundary Integral (variable permeability)

### Data Generation

As outlined in section 4 (last paragraph) in addition to the surface discretisation a volume discretisation is required for non-linear problems. In the present program this was achieved by generating a continuous mesh of tetrahedra within a set of hexahedra which modelled the problem, using an automatic procedure.

Bending Magnet Type 1

For this test a magnet exhibiting considerable non-linear behaviour was used. The Rutherford Laboratory Type 1 bending magnet[18] shows 17% departure from linearity of central field at 1.58T(450A). The magnet is fabricated from two different steels and is an 'H' configuration (Figure 8) with a salient pole. Results at 450A are shown in Figure 9 together with a comparison with GFUN3D.[5]

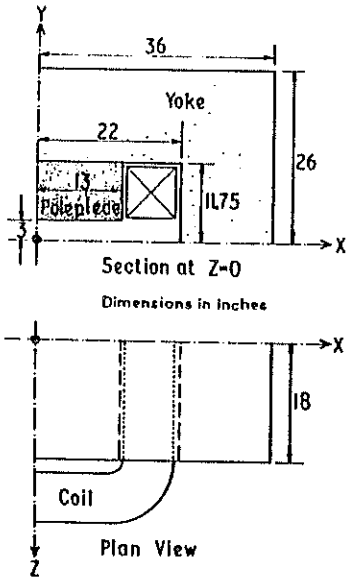


FIG. 8 OCTANT OF BENDING MAGNET TYPE 1

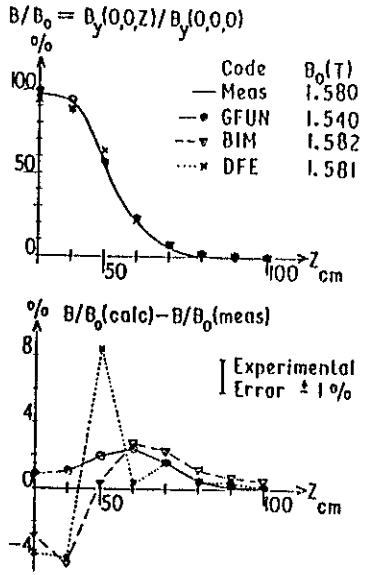


FIG. 9 COMPARISON OF VARIOUS ALGORITHMS WITH MEASUREMENTS FOR BENDING MAGNET TYPE 1

Differential Finite Element (Variable permeability)

Data Generation

The theoretical results presented in section 3 were used as the basis of a three dimensional program. Iso-parametric elements of the 'serendipity' type[15] were selected and element (stiffness) coefficients (3.7) and boundary forces (3.8) were computed by Gaussian quadrature. Magnets for solution are modelled by a mesh of elements generated by the automatic subdivision of hexahedra. The system of equations (3.6) were solved by applying the method of incomplete Choleski Decomposition with Conjugate Gradients (ICCG).[19] A simple iterative method is used for non-linear problems.

Bending Magnet Type 1

To achieve a valid comparison with the integral method this magnet was also used to test the Differential Finite Element program. The measured and computed results are shown in Figure 9.

Window-Frame Gradient Magnet

An example of the use of the boundary integral method is the high-resolution spectrometer magnet for Oxford University which is currently being designed at Rutherford Laboratory. The main features of the magnet are that it will provide a dipole field from 0.3T to 1.3T over a sector of 100° on a central orbit radius of 1.6m. The primary focussing is achieved by a tapered gap in the dipole which gives a field gradient. In order to minimise the aberrations the input face of the magnet will be fitted with an extension ("Bay Window"), consisting of an approximately circular segment of iron projecting from below the coils. In order to study how the dipole/gradient field inside the magnet blends with the 'bell shaped' field under the bay window a model of a straight magnet has been set up for analysis by the linear boundary integral program, see Figure 10. Figure 10 also shows the contours of normalised fields in the vicinity of the bay window, from which the transition from the gradient regime to the bell shape can be clearly seen.

## 6. CONCLUSION

The theory and some preliminary results from two new three-dimensional (non-linear) computer programs have been presented. One program uses an integral formulation (BIM) in which only iron regions are discretised - for linear problems this is reduced further to a surface discretisation. The other code is based on a differential formulation (DEM) and requires a continuous mesh throughout space. Both codes use a magnetic scalar potential so that there is only one unknown at each mesh point and, furthermore, the total scalar potential is used in iron regions thus ensuring a numerically stable solution.

The integral variant can be seen as a logical extension to the magnetisation vector integral equation code (GFUN) with a scalar function as independent variable and options on the order of base functions giving an expected improvement in economy and accuracy. For linear problems the requirement that surfaces only

need subdividing into elements leads to further increases in efficiency and accuracy. The results achieved for the bending magnet BM105 confirm this and allow the design of high resolution magnets to proceed purely by computational methods. Whilst the non linear version is not yet as highly developed as the corresponding linear version, ie only first order elements have been included so far, a dramatic gain in accuracy is to be expected when the second order element is introduced.

The differential variant is an extension to the work discussed in reference 16 utilizing two scalar potentials. The preliminary results have demonstrated the viability of this approach for three dimensions and that the accuracy on field shape will improve considerably when the level of discretisation is increased and higher order elements are introduced. It is interesting to note that the source field is only calculated at points on the interface between the two regions, which can be any convenient surface (not necessarily the iron surface) satisfying the condition that it spans the region of space containing the iron and does not contain currents.

TABLE 1

INTEGRAL VERSUS DIFFERENTIAL

| FEATURE | INTEGRAL | DIFFERENTIAL (FEM) |
|---|---|---|
| 1.DISCRETISATION | Relatively straightforward (iron only, surface only for linear problems). | Difficult. Whole of problem space with continuous mesh of elements. |
| 2.EXTERNAL (INFINITE SPACE) FOR FIELD BOUNDARY CONDITION | Automatically taken into account by the formulation. | Requires external boundary conditions to be placed sufficiently far away or the use of special infinite elements as in Coupled Finite Element and Boundary Integrals[20] alternatively the use of ballooning finite elements[21]. |
| 3.GALERKIN/ VARIATIONAL | Expensive to apply because of multiple integrals | Easy to apply and intrinsic to formulation |
| 4.MATRIX | Fully populated, expensive to compute and to make symmetric. Solution time $O(n^3)$. | Sparse, symmetric and cheap to compute. Solution time $O(n^2)$. |
| 5.RECOVERY OF FIELDS | Accurate but expensive. | Difficult to achieve smooth accurate results unless extra processing employed |

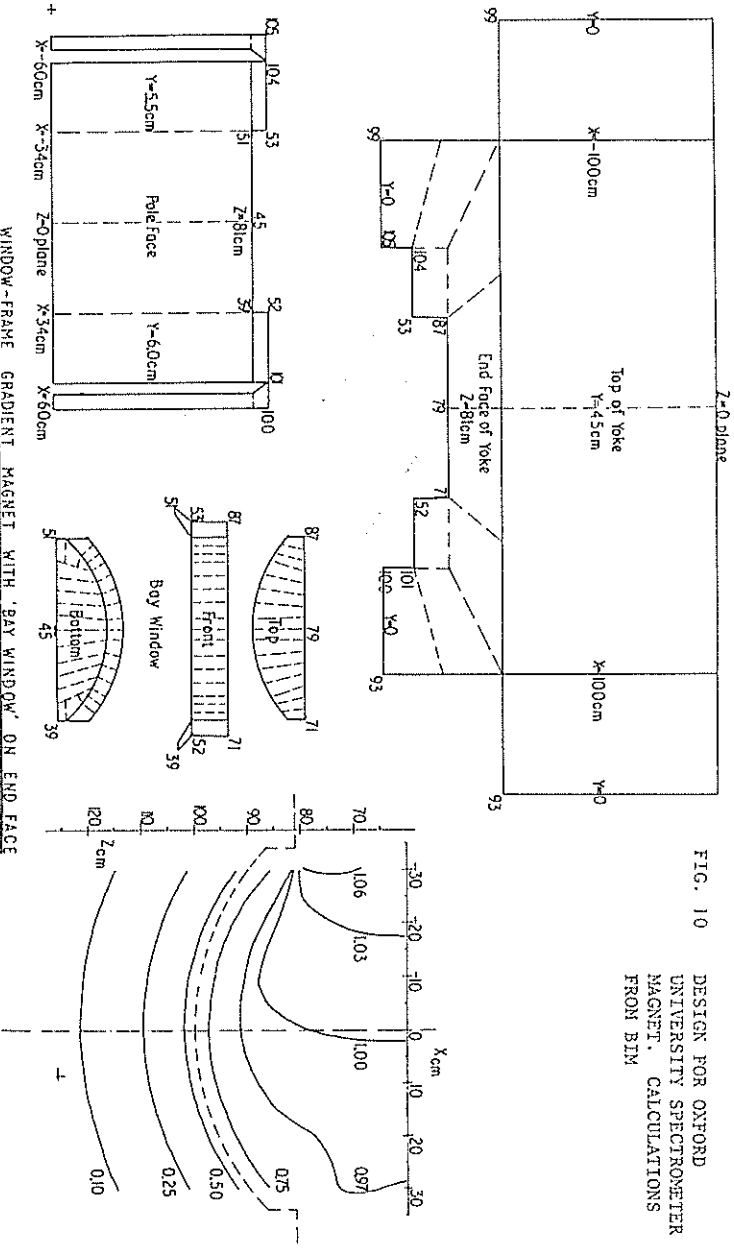


FIG. 10 DESIGN FOR OXFORD UNIVERSITY SPECTROMETER MAGNET. CALCULATIONS FROM BIM

TABLE 2

COMPUTER STATISTICS FOR TYPE I
BENDER MAGNET IBM(360/195)

| CODE | TOTAL TIME MINUTES | CORE KILO BYTES | NUMBER OF EQUATIONS | MAX. ERROR ON SHAPE |
|---|---|---|---|---|
| GFUN | 13<br>65 | 660<br>660 | 540<br>1080 | 3%<br>2% |
| BIM | 23 | 800 | 392 | 4% |
| DEM | 6<br>12 | 270<br>310 | 1000<br>1900 | 8%<br>6% |

The development of these two computer programs provide useful tools for investigating the relative merits of integral and differential methods. The intrinsic features of the two formulations are summarised in Table 1, and some statistics for the results given in Figures 7 and 8 are presented in Table 2. It is not possible at this stage to arrive at a definitive conclusion as to which is the most efficient. However, it is projected that for the type of problem and accuracies considered here the two methods will be equally expensive. The problem geometry and accuracy required will determine which method is more attractive. It is still difficult to form a continuous mesh over all space and until this problem is solved integral formulations will remain very attractive.

## 7. ACKNOWLEDGEMENTS

The authors are indebted to the following members of Rutherford Laboratory Staff: D B Thomas, N J Diserens, M Newman, and C Biddlecombe for their helpful advice during the course of this work and to Mrs P Morgan for preparing the typescript. Also to R Lari of the Argonne National Laboratory for supplying the measurements on Magnet BM105 and to Ch Iselin of CERN for many helpful discussions.

## 8. REFERENCES

1. Winslow, A A. Numerical Solution of the Quasi-Linear Poisson Equation in a Non-Uniform Triangular Mesh. J Comp Phys Vol.1, pp. 149-72, 1967.

2. Chari, M W K and Silvester, P. Finite Element Analysis of Magnetically Saturated dc Machines. IEEE Trans Power Apparat Syst Vol. PA-90, p 2362, 1971.

3. Newman, M J, Trowbridge, C W and Turner, L R. Proc 4th Int Conf on Magnet Technology, Brookhaven, 1972.

4. Collie, C J, Diserens, N J, Newman, M J, Trowbridge, C W. Progress in the Development of an Interactive Computer Program for Magnetic Field Design and Analysis in Two and Three Dimensions. RL-73-077 (Rutherford Laboratory, 1973).

5. Armstrong, A G A M, Collie, C J, Diserens, N J, Newman, M J, Simkin, J, Trowbridge, C W. New Developments in the Magnet Design Program GFUN, RL-75-066 (Rutherford Laboratory 1975).

6. Collie, C J. Magnetic fields and potential of linearly varying current or magnetisation in a plane bounded region. Proc COMPUMAG Conf, Oxford 1976.

7. Simkin, J, Trowbridge, C W. Magnetostatic Fields Computed using an Integral Equation derived from Green's Theorems. RL-76-041,(Rutherford Laboratory, 1976).

8. Trowbridge, C W. Applications of integral equation methods for the numerical solution of magnetostatic and eddy current problems. Proc. Int. Conf. on Numerical Methods in Electrical and Magnetic Field Problems, Santa Margherita, Italy, 1976. (Also RL-76-071 (1976)).

9. Polak, S J, Watchers, A, De Beer, A. An account of the use of the finite element method for magnetostatics. Proc COMPUMAG Conf, Oxford, 1976.

10. Iselin, Ch. A Scalar Integral Equation for Magnetostatic Fields. Proc COMPUMAG Conf, Oxford, 1976.

11. Wolff, W, Muller, W. General numerical solution of the magnetostatic equations. Wiss Ber AEG-TELEFUNKEN 49 (1976) 3, p.77.

12. Zienkiewicz, O C, Lyness, J and Owen, D J R. Three-Dimensional Magnetic Field Determination using a Scalar Potential. IEEE Transactions on Magnetics, Vol Mag. 13, No. 5, September 1977.

13. Zienkiewicz, O C, et al. The Couplings of the Finite Element and Boundary Solution Procedures. Int. J. for Numerical Methods in Engineering. Vol 11, 355, 375, 1977.

14, Jeng, G, Wexler, A. Isoparametric, finite element, variational solution of integral equations for three-dimensional fields. IJNME, Vol.11, p. 1455, 1977.

15. Zienkiewicz, O C. The Finite Element Method in Engineering Science. McGraw-Hill, 1971, 3rd Edition 1978.

16. Simkin, J, Trowbridge, C W. Which Potential, A comparison of the various scalar and vector potentials for the numerical solution of the non-linear Poisson problem. RL-78-009/ B 1978. To be published IJNME

17. Lari, R J. Report RJL-6: Magnetic Measurements of Bending Magnets BM-105 and BM-106. Argonne National Lab, 1965. R J Lari. Private communications.

18. Newman, M J. Private Communication. Ritchie,P J S, Loach, B G. Nimrod Beam Line Equipment Data Handbook. Rutherford Laboratory, 1968.

19. Meierink J A and v.d. Vorst, H A. An iterative solution matrix for linear systems of which the coefficient matrix is a symmetric M-matrix. Mathematics of Computation, January, 1977.

20. Zienkiewicz, O C, et al. The coupling of the finite element and boundary solution procedures. Int. J. for Numerical Methods in Engineering, Vol 11, 355, 373, 1977.

21. Silvester, P P, Lowther, D A, Carpenter, C J, Wyatt, E A. Exterior Finite Elements for 2D field problems with open boundaries. Proc. I.E.E, Vol 124, pp 1267-1270, 1977.

# CALCULATION OF THE MAGNETIC FIELD OF THE ISOCHRONOUS CYCLOTRON SECTOR MAGNET BY THE INTEGRAL EQUATION METHOD

P.G.Akishin, S.B.Vorozhtsov, E.P.Zhidkov

Joint Institute for Nuclear Research, Dubna, USSR

At the Laboratory of Nuclear Problems, JINR, a possibility of the construction of a powerful neutron source with a neutron beam energy of 14 MeV and a flux of $10^{14}$–$10^{15}$ n/(cm$^2$, sec) is investigated. The ring isochronous cyclotron with a 35 MeV deutron energy and a 10–100 mA beam current will be the main accelerator facility for producing the above-mentioned neutron flux. The radial-sector structure with a four-fold symmetry is conceived for the cyclotron.

The calculational results of the magnetic field of the cyclotron magnet are given in the report. Figure 1 shows the upper view of the calculational magnet model along with the sector current coil. The air gap height of the magnet is 5 cm, whereas the ratio of the maximum pole length to the gap height is about 30. The external diameter of the four sector system including the yoke is 8 m. The magnetic field value in the air gap is about 18 kGs. The field has been calculated using the computer code MAGSYS by solving a 3-dimensional vector integral equation for the magnetic field induction[2-3]. The magnet body volume has been considered as a set of triangular prisms or parallelepipeds. The values of the induction vector and the magnetic permeability have been assumed to be constant inside the above said regions. The embedding method[4] has been used to solve the nonlinear algebraic system, which approximated the vector integral equation under above conditions. The resulting algebraic system is as follows:

$$B_{mn} - \sum_{i=1}^{M} \left(1 - \frac{1}{\mu_i}\right) \sum_{j=1}^{3} f_{ij}^{mn} B_{ij} = \psi_{mn} \qquad (1)$$

where $m = 1,2,3, \ldots, M$, $n = 1,2,3$. $\mu_i = f\left(\sum_{j=1}^{3} B_{ij}^2\right)$ is a magnetic permeability, $f_{ij}^{mn}$ – is a field induction independent function, $\psi_{mn}$ is a given function of coordinates.

An abbriviated form of equation (1) is given by

$$A \vec{x} = \vec{b},$$

where the elements of the matrix $A$ are functions of the solution vector $\vec{x}$. Consider, that the relation

$$\mu(t) = 1 + [\mu(1) - 1] \cdot t \qquad (3)$$

takes place under the condition $0 \le t \le 1$. Then the vector $\vec{x}$ is a function of the parameter $t$ and the solution of equation (2) is reduced to that of the Cauchy problem with the initial value $\vec{x}(0) = \vec{b}$. The calculation has been made with a constant step of the parameter $t$ and with the recalculation of the initial $\vec{x}_0$-value for the $t = t_n$ according to the expression

$$\vec{x}_0(t_n) = 2\vec{x}(t_{n-1}) - \vec{x}(t_{n-2}). \qquad (4)$$

The solution was improved at every $t_n$ using the iterative formula

$$\vec{x}_{k+1} = \vec{x}_k + \alpha\left(A_{kn}\vec{x}_k - \vec{b}\right), \qquad (5)$$

where the $\alpha$-value is given by

$$\alpha = -\gamma \frac{\left(A_{kn}\vec{x}_k - \vec{b},\ A_{kn}\left[A_{kn}\vec{x}_k - \vec{b}\right]\right)}{\left\| A_{kn}\left(A_{kn}\vec{x}_k - \vec{b}\right)\right\|^2} \qquad (6)$$

to obtain the maximum convergence rate of the process. In expression (6) it is assumed that

$$\| A_{k+1,n} \| \approx \| A_{k,n} \|. \qquad (7)$$

Condition (7) was provided with the help of the factor $\gamma \le 0.2$. In the calculations it sometimes occurred that the magnitude of $\alpha$ tended to zero at some values of $t_n$. In this case instead of eq. (5) we used the expression

$$\vec{x}_{k+1} = \vec{x}_k + \vec{D}_k, \qquad (8)$$

where the vector $\vec{D}_k$ could be defined from the conditions

$$\left(\vec{D}_k, \left[A_{kn}\vec{x}_k - \vec{b}\right]\right) = 0, \qquad (9)$$

$$\| \vec{D}_k \| = \| A_{kn}\vec{x}_k - \vec{b} \|. \qquad (10)$$

From our point of view, the main advantage of the used method for solving the algebraic system is a possibility to have a converging process in all calculations performed

by the authors. The convergence takes place even for the magnet with a "bad" [5] partition of the magnet volume into subregions. Other advantages are a possibility to keep in the computer core storage only a part of the system matrix and central processor execution time which is comparable with that of the GFUN3D code [2] when running jobs at the CDC 6500.

The sector magnet was calculated with a various number of the subregions of constant magnetization. The maximum number was 192 subregions which was equivalent to the 576 x 576 algebraic system. The best results obtained for the triangular prism partition (Fig. 1) are presented by dashed lines in Figs. 2-4. The solid lines present the magnetic field measurement data for the 1 : 7 model of the magnet. As one can see in Fig. 6 the difference between the experimental and calculated data is about 0.5% for the azimuthally mean field, 5% for the flutter, 2% for the amplitude of the main harmonic in the radial range R = 15-28 cm. Near the minimum and the maximum radial position of the observation point the deviations of the calculated curves from experimental ones are largest due to the strong nonuniformity of the pole field in the vicinity of these regions. The assumption of the piece-wise constant magnetization distribution in these parts of the pole are least valid.

The evaluation of the magnet field using an other method and based on it a magnet model design has been made it possible to obtain the discrepancy between the measured mean field $B_0$ and the required isochronous field $B_R$ in the range of 10% (Fig. 4). As seen from Fig. 4 the application of the described calculations could improve considerably the accuracy of the $B_0$ evaluation apart from the pole ends.

As a final remark the authors wish to thank Dr. N.L.Zaplatin and Mr. N.A.Morozov for providing the magnetic field measurement data of the magnet model.

References

1. Yu.M.Ado et al. Proc. of the Fifth All-Union Conf. on Char. Part. Acc. Dubna, 1976, v.II, p.317.
2. C.W.Trowbridge et al. GFUN3D user guide, RL-76-029/A .
3. P.G.Akishin, S.B.Vorozhtsov, E.P.Zhidkov. D10,11-11264, Dubna, 1978, p.214.
4. J.Casti, R.Kalaba. Imbedding Method in Applied Mathematics, Addison-Wesley Publishing Company, 1973.
5. A.G.A.Armstrong et al. Proc. of the Fifth Int. Conf. on Mag. Tech. Roma, 1975, p.168.

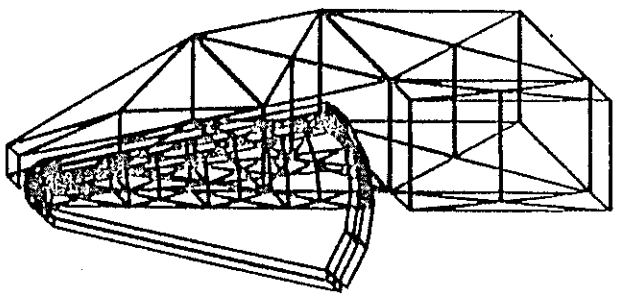

Fig. 1. A display representation of the sector magnet (the upper view).

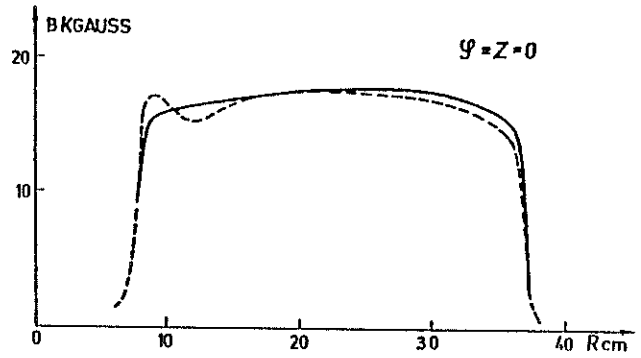


Fig. 2. A "hill" field performance.

a)

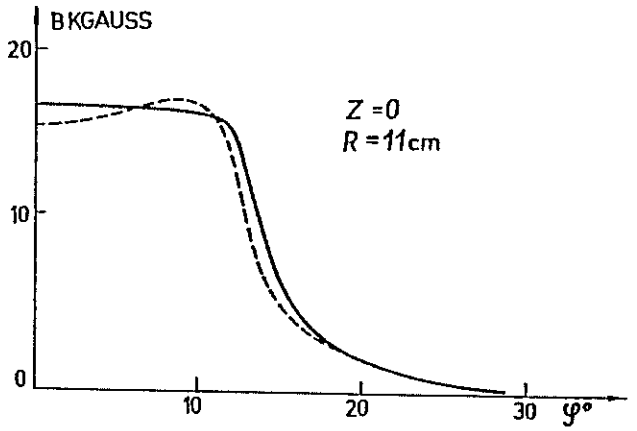


в)

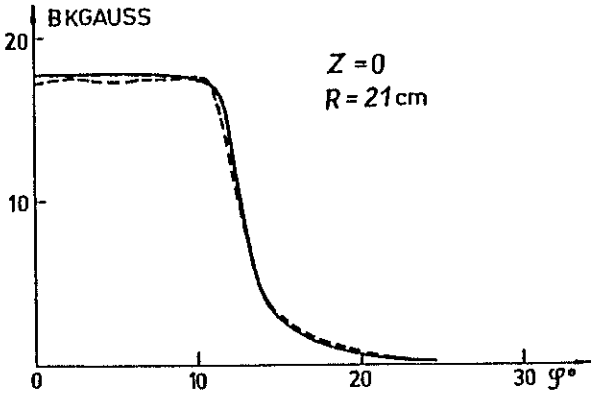

c)

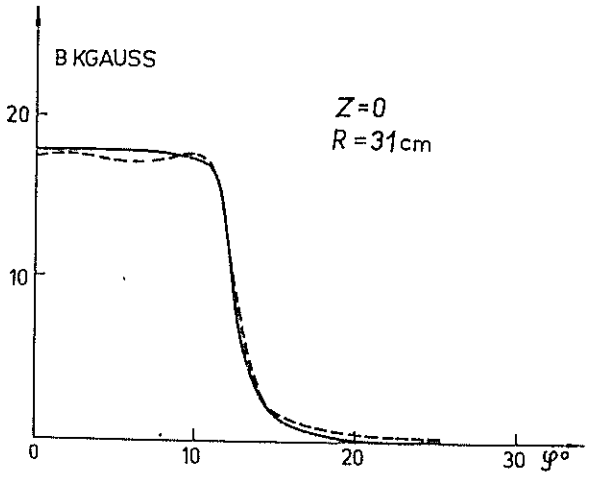


Fig. 3. An azimuthal distribution of the field.

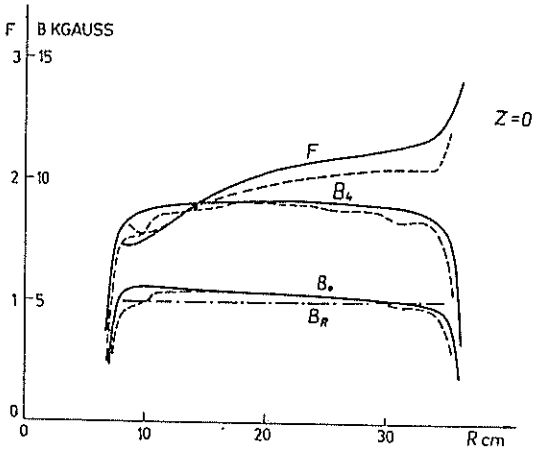


Fig. 4. Results of the harmonic analysis of the field.

# INTEGRAL METHODS FOR THE CALCULATION OF MAGNETIC FIELDS IN TURBOGENERATORS

R.J. Jackson
Central Electricity Research Laboratories,
Leatherhead, Surrey KT22 7SE

## ABSTRACT

This paper considers the use of integral methods for the calculation of magnetic fields in turbogenerators. Using an integral method the magnetic field is taken to arise from a set of field sources representing both the generator windings and the non-linear magnetisation of the rotor and stator iron.

The solution of the two dimension problem of the calculation of magnetic fields in the active region of the turbogenerator is described. It is shown that the number of elements required to represent the complex geometry of the rotor and stator iron can be considerably reduced by a suitable choice of magnetisation pattern within an element. The evaluation of the magnetisation of the elements is further simplified by the representation of the field vector in terms of a type 1 and type 2 field, which correspond to the spatial harmonics of magnetic field rather than the radial and azimuthal components of the magnetic field. Results of a computer program based on this analysis are given.

The use of this method for the calculation of magnetic fields in three dimensions is then considered. Preliminary work is described in which the fields are calculated for the simplified core geometry of the slotless generator and are compared with field measurements taken on a model generator.

## 1. INTRODUCTION

An important part of the design of large turbogenerators is the calculation of the magnetic fields in the generator windings and the stator core. Figure 1 shows a cross section of a typical two-pole generator. In the centre there is a steel rotor with slots in the outer surface carrying the field windings. The stator core is constructed from silicon steel laminations with slots in the inner surface supporting the armature windings. The rotor revolves at 50 Hz and the armature winding carries a three-phase a.c. current which produces a rotating dipole field.

Although much of the winding m.m.f. is dropped across the generator airgap the magnetic flux density in the rotor and stator cores is high, and the saturation of the core steel significantly affects the overall generator field. The stator core is laminated to limit the eddy currents due to the main generator flux but near the ends of the generator the axial magnetic fields (normal to the plane of the laminations) induce currents in the stator core. Thus the calculation of the generator magnetic fields requires a three-dimension, time-dependent field program which includes the effects of saturation and eddy currents.

It has been found that general purpose programs are not able to represent the complex geometry of the rotor and stator iron in sufficient detail. Thus special programs have been developed for the calculation of the electromagnetic fields in electrical machines. In such programs approximations are made to reduce the number of elements required to represent the generator, thus allowing a detail representation of regions of specific interest such as the teeth and screen and end windings.

The program SLAMED[1] uses a boundary value method to calculate the magnetic fields and eddy currents in the end region of the stator core. Since the initial formulation of this program, analysis of measurements of the magnetic fields in large generators has shown that the field in the airgap can be conveniently described as the interaction of a set of sources of magnetic field[2].

This, together with the known accuracy of integral field programs for magnetostatic problems[3], suggests a new approach to the computation of generator magnetic fields, in which the magnetic fields outside the stator core and end screen are assumed to depend only on the

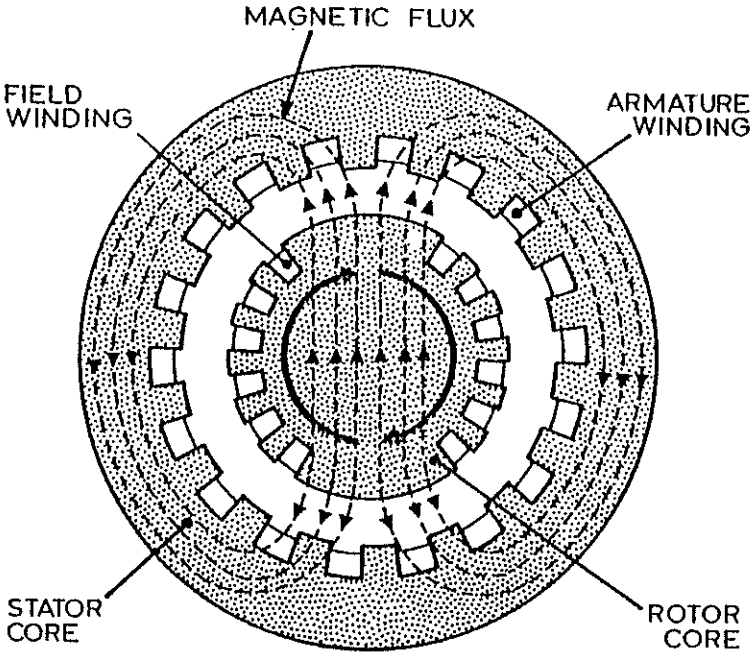


FIG.1 A CROSS SECTION OF THE GENERATOR

armature and field winding currents, and the radial and tangential magnetisation of the rotor and stator core. If this is the case then the calculation of the fields outside the generator is a magnetostatic problem and may be solved using a standard integral method. The effects of the axial magnetisation of the rotor could be included in this calculation should it prove necessary but this would increase the size of the problem.

The stator core is laminated and therefore its axial permeability is almost constant: being limited by the proportion of iron in the laminate (the stacking factor). Thus the axial fields and eddy currents in the stator core and end screen can, in principle, be calculated using a linear boundary value method in which the eddy currents are represented by a single stream function[1]. Although measurements of the fields outside the stator core show that the magnetic fields vary little with frequency and therefore the eddy currents induce only low fields outside the core, this artificial division of the problem is a leap of faith which can be tested only by comparison of computed and measured fields.

This paper considers the first part of the problem, the use of integral methods to calculate the magnetic fields outside the stator core.

## 2. THE FIELDS OUTSIDE THE STATOR CORE

To calculate the magnetisation of the rotor and stator, the core steel is divided into a number of blocks (each with a fixed magnetisation) and a magnetic interaction matrix is defined to relate the magnetisation of each block to all other blocks. This matrix can be expressed in the form:

$$\underline{B}_i = \mu_o \underline{H}_i + \underset{\sim}{M}_{ij}\, \underline{m}_j \qquad \ldots (1)$$

where $\underline{B}_i$ is the magnetic flux density vector at the centre of the ith block and $\underline{H}_i$ is the magnetic field vector at the same point due to the generator windings. $\underset{\sim}{M}_{ij}$ is a tensor defining the flux density at the centre of the ith element due to a unit magnetisation in the jth element, and $\underline{m}_j$ is the magnitude of the magnetisation in the jth element. N.B. The Einstein summation convention is assumed.

As in SLAMED[1], the time varying magnetic fields and permeability are represented by the first and third time harmonics of the rotor frequency, the corresponding terms for the permeability being the zeroth and second harmonics. In addition, the variation of the magnetisation across a phase band of the armature winding is neglected; all blocks in the same position within the span of a tooth, therefore, have a related (phase shifted) magnetisation. Thus the variation of magnetisation within the span of a tooth is represented in detail, but the variation from tooth to tooth is represented only by the first and third spatial harmonics.

To simplify the representation of the rotor and stator core the elements (which now represent a set of blocks) are sectors of a cylinder. Each element has two independent magnetisation patterns for each time harmonic which vary across the element in a way typical of the fields in the generator core. The type 1 magnetisation (see figure 2) is characteristic of the rotor core and the type 2 is characteristic of the stator core. Thus the magnetisation of a single element is specified by four complex scalars representing the magnitude of the four unit magnetisation patterns:

$$\hat{m}_1^{(1)} = \exp j(\theta + \omega t)\, \hat{\underline{r}} + j \exp j(\theta + \omega t)\, \hat{\underline{\theta}}$$

$$\hat{m}_2^{(1)} = \frac{\rho^2}{r^2} \exp j(\theta + \omega t)\, \hat{\underline{r}} - j \frac{\rho^2}{r^2} \exp j(\theta + \omega t)\, \hat{\underline{\theta}} \qquad \ldots (2)$$

$$\hat{m}_1^{(3)} = \frac{r^2}{\rho^2} \exp 3j(\theta + \omega t)\, \hat{\underline{r}} + j \frac{r^2}{\rho^2} \exp 3j(\theta + \omega t)\, \hat{\underline{\theta}}$$

$$\hat{m}_2^{(3)} = \frac{\rho^4}{r^4} \exp 3j(\theta + \omega t)\, \hat{\underline{r}} - j \frac{\rho^4}{r^4} \exp 3j(\theta + \omega t)\, \hat{\underline{\theta}}$$

where $\rho$ is the mean radius of the element, the subscripts denote a type 1 and type 2 magnetisation pattern and the superscripts the time harmonics.

Using these expressions, the curl of the magnetisation is zero, so the magnitude of the field source representing a block of iron can be expressed as an integral of the surface currents. Also the diverg-

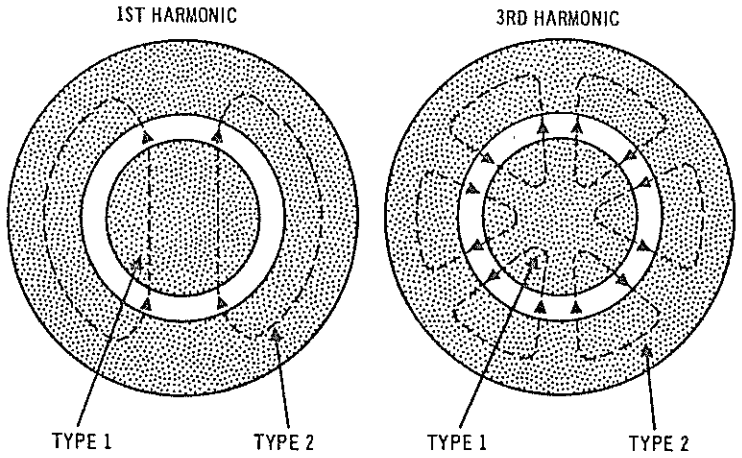


FIG. 2 THE MAGNETISATION PATTERNS

ence of the magnetisation is zero, allowing the use of relatively large elements in regions of the core where the permeability is uniform.

To calculate the magnetisation of the rotor and stator core a zeroth and second harmonic permeability vector is defined where:

$$\Lambda_i^{(n)} = \int_0^{2\pi/\omega} \frac{\mu(\underline{m}_i\ (t))}{\mu(\underline{m}_i\ (t)) - 1} \exp\ (-jn\omega t)\ dt \qquad \ldots\ (3)$$

Substituting for the flux density vector in equation (1) the calculation of the magnetisation vector is formulated as a pair of matrix equations:

$$\begin{bmatrix} m_{ri}^{(1)} \\ m_{0i}^{(1)} \end{bmatrix} = \begin{bmatrix} \Lambda_i^{(o)}\ \delta_{ij} - M_{r1ij}^{(1)} & -M_{r2ij}^{(1)} \\ -M_{01ij}^{(1)} & \Lambda_i^{(o)}\ \delta_{ij} - M_{02ij}^{(1)} \end{bmatrix}^{-1} \times \begin{bmatrix} \mu_o\ H_{rj}^{(1)} \\ \mu_o\ H_{0j}^{(1)} \end{bmatrix}$$

and $\qquad \ldots\ (4)$

$$\begin{bmatrix} m_{ri}^{(3)} \\ m_{0i}^{(3)} \end{bmatrix} = \begin{bmatrix} \Lambda_i^{(o)}\ \delta_{ij} - M_{r1ij}^{(3)} & -M_{r2ij}^{(3)} \\ -M_{01ij}^{(3)} & \Lambda_i^{(o)}\ \delta_{ij} - M_{02ij}^{(3)} \end{bmatrix}^{-1} \times \begin{bmatrix} \mu_o\ H_{rj}^{(3)} - \Lambda_j^{(2)}\ m_{rj}^{(1)} \\ \mu_o\ H_{0j}^{(3)} - \Lambda_j^{(2)}\ m_{0j}^{(1)} \end{bmatrix}$$

The magnetisation of the non-linear rotor and stator steel is evaluated by an iterative procedure in which the permeability vectors are set and the first and third harmonic magnetisation vectors calculated; these values are then used to update the permeability vector and so on.

## 3. THE FIELDS IN THE ACTIVE REGION OF THE GENERATOR

For the first test program a two dimensional problem was considered: the calculation of the magnetic fields in the active (central) region of the generator. This problem provides a good test of the approach to be used for the full three dimensional program.

Because the terms of the interaction matrix are calculated from surface currents any inaccuracy in their computation will appear as additional currents at the boundary of the element. This introduces a discontinuity in the magnetic flux parallel to the boundary between adjacent elements if there is a suitable circuit for the rotation of magnetic flux within the core. For example, if the core back is divided radially into two elements, any additional surface currents will produce a loop of magnetic flux within the core back. The effect of these additional surface currents is reduced by the introduction of an additional narrow element (representing the butt joints between laminations). Since this element has a common boundary with both elements the only path for circulating magnetic fluxes is a high reluctance path through all three elements. This empirical approach has been found to work well in practice.

To simplify the calculation of the terms of the interaction matrix (for two dimensional problems) it is convenient to work in terms of a type 1 and type 2 magnetic field rather than the radial and tangential magnetic fields, where:

$$B_1 = \tfrac{1}{2}\ (B_r - j\ B_\theta) \quad \text{and} \quad B_2 = \tfrac{1}{2}\ (B_r + j\ B_\theta)$$

Using these field components the type 1 magnetic field outside an element with a unit type 1 magnetisation is zero and constant ($\frac{1}{2}$) inside the element and similarly the type 2 field produced by an element with a type 2 magnetisation is zero outside and constant ($\frac{1}{2}$) inside the element.

The two dimensional program converges rapidly (typically in four steps) to give a stable solution. Figure 3 shows the calculated flux density at the inner surface of the stator core demonstrating one advantage of the integral method, the simple representation of the

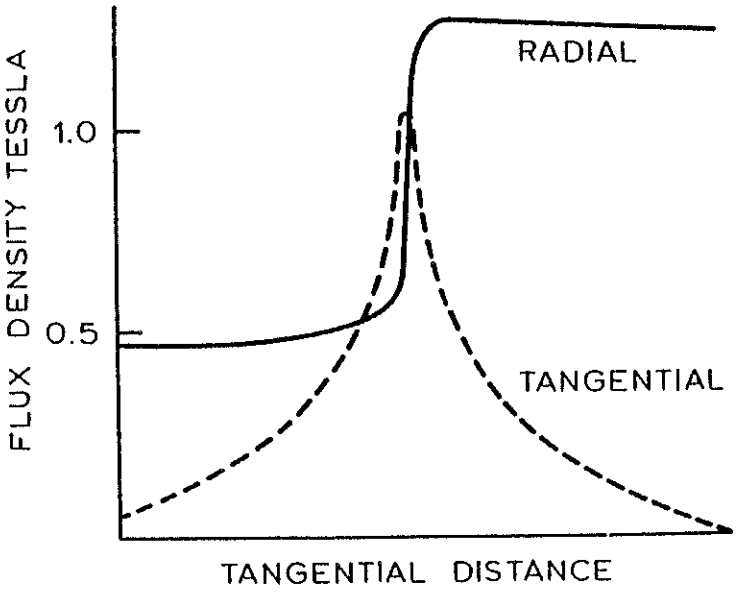


FIG.3 FLUX DENSITY AT THE TOOTH TIP

corners of the core. In table 1 the calculated fields and generator voltage are compared with measurements taken on a typical 660 MW generator. Reasonable agreement (within 2%) is shown for most parameters with the exception of the generator load angle. Because the saliency (lack of quadrature symmetry) of the rotor was neglected in this test program, the calculated load angle was less than the measured value. The program has since been reformulated to include the effect of rotor saliency.

Table 1: The Generator Fields

| | Measured | Calc. | Measured | Calc. | Calc.* |
|---|---|---|---|---|---|
| Rotor current kA | 1.61 | 1.61 | 3.3 | 3.3 | 3.3 |
| Stator current kA | 0 | 0 | 15.4 | 15.4 | 15.4 |
| Terminal voltage kV | 23.5 | 23.4 | 24.3 | 24.3 | 24.5 |
| Phase angle | - | - | $1.0^{o}$ | $1.4^{o}$ | $1.2^{o}$ |
| Load angle | - | - | $61^{o}$ | $55^{o}$ | $55^{o}$ |
| Radial flux density at the tooth tip | 1.271 | 1.240 | 1.290 | 1.284 | 1.296 |

*at the overlap between adjacent phases of the armature windings.

Generally the fields were calculated at the centre of the stator winding phase band but to estimate the variation of magnetisation across a phase band the fields were also calculated at the overlap between adjacent phases. The voltage and flux density differed by about 1% in the two cases. In practice less than half the stator elements lie at the overlap between phase bands so neglecting the variation of magnetisation across a phase band should introduce relatively small errors in the calculated fields and voltages.

## 4. THE FIELDS IN THE GENERATOR END REGION

Analysis of measurements of the axial magnetic fields in the airgap of a 500 MW generator by Minors[2] showed that the field can be represented as the sum of three field vectors. Figure 4 shows a section of the generator end region and a vector diagram representing the axial flux density.

The two vector components which result from the magnetisation of the rotor and stator cores are in phase with the radial flux in the airgap and at constant voltage are independent of the generator load conditions. The third component which results from the magnetisation of the rotor end by the field windings is in phase with the rotor axis. Hence the axial flux density is a simple function of generator load angle. Figure 4 shows the expected linear relationship between the square of axial flux density and the cosine of generator load

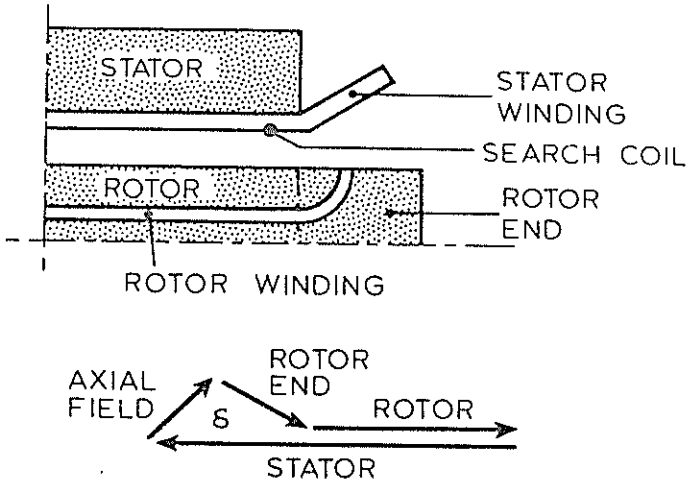


FIG.4 AXIAL FIELD IN THE AIR GAP

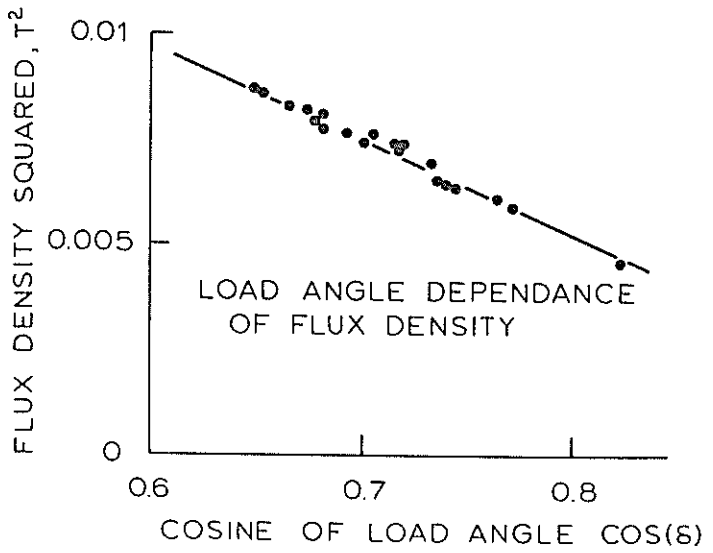

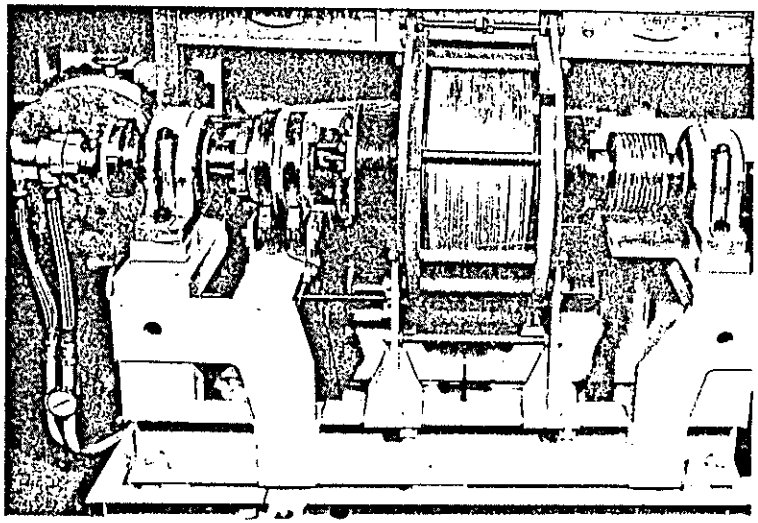

FIG. 5 THE SLOTLESS GENERATOR RIG

angle. These results suggest that the axial magnetic fields in the generator airgap are due to the magnetisation of the rotor and stator cores and that these magnetisations could be represented by relatively few, well chosen, elements.

To study the fields in the generator end region a test program was written to model the fields in the end region of the slotless generator[4] and the results compared with measurements taken on a laboratory model of the generator (figure 5). The rotor and stator cores are smooth cylinders and the field winding is a water cooled, saddle winding clamped on to the rotor surface by a carbon fibre hoop[5]. The mesh representing the generator is shown in figure 6. For the calculations the rotor and stator core is divided into ten cylindrical elements. The preliminary results in figure 7 show reasonable agreement with measurements of the radial and axial flux density taken in the generator airgap and over the generator end windings. These measurements were taken at a low rotor frequency (5 Hz) reducing the effects of the eddy currents in the stator core.

There is some anomolous variation of the radial flux density near the end of the stator core. Further work is required to see if this is the result of using a coarse mesh or because the axial magnetisation of the rotor core was neglected.

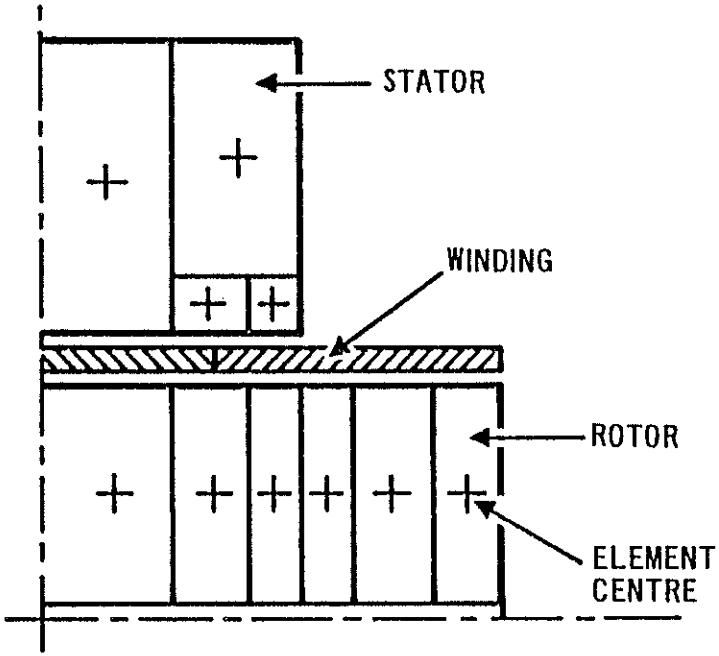


FIG.6 THE GENERATOR MESH

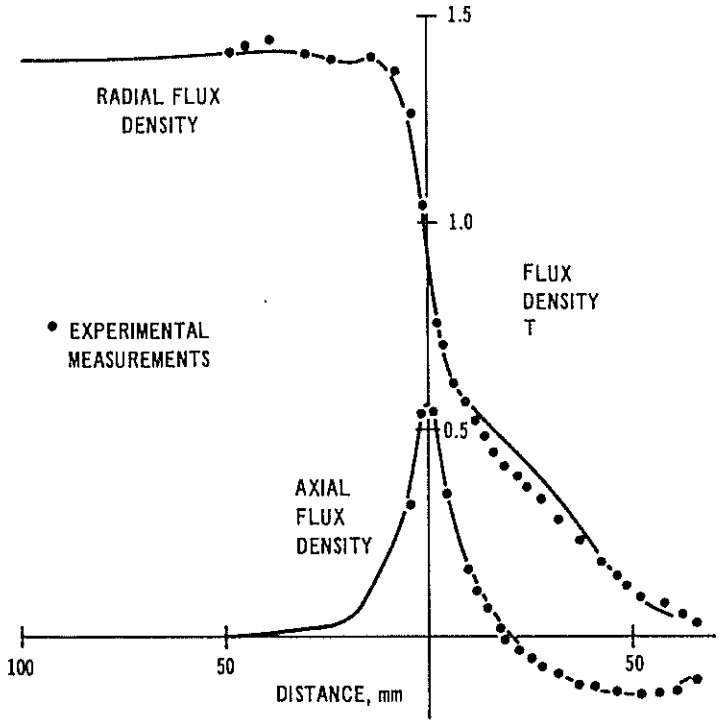


FIG 7 FIELD IN THE GENERATOR AIRGAP

## 5. CONCLUSIONS

Specialist field programs can be devised for the calculation of the magnetic fields in electric machines using integral methods. A careful choice of the shape of the elements and the magnetisation pattern within an element should allow the rotor and stator cores to be represented by relatively few elements. This would simplify both the computation of the fields and show more clearly the influence of the principle design features on the magnetic fields in the generator.

## 6. ACKNOWLEDGEMENTS

The work reported here was carried out at the Central Electricity Research Laboratories and is published with the permission of the Central Electricity Generating Board.

## 7. REFERENCES

1. Jacobs, D.A.H., Minors, R.H., Myerscough, C.J., Rollason, M.J. and Steel, J.G., Calculation of losses in the end region of turbogenerators. Proc. IEE, 124 (4), pp.356-362, 1977.

2. Minors, R.H., Core end heating in turbogenerators: the importance of load angle. CERL Laboratory Note RD/L/N 172/74, 1974.

3. Collie, C.J., Diserens, N.J., Newman, M.J. and Trowbridge, C.W., Progress in the development of interacting computer programs for magnetic field analysis in two and three dimensions. Rutherford High Energy Lab. Report rl-73-077, 1976.

4. Spooner, E., Airgap-wound alternators for large-scale power generation. PhD Thesis, University of Aston in Birmingham, 1972.

5. Everest, D.J., Muhlhaus, J. and Roberts, I., The CERL Prototype Slotless Generator. CERL Laboratory Note RD/L/N 57/76, 1976.

# A COMPARISON OF TWO METHODS OF FIELD SOLUTION FOR SLOTTED BOUNDARY SHAPES IN TWO DIMENSIONS

K.J. Binns, P.A. Kahan, G.R. Rees, J. Simkin and C.W. Trowbridge,
University of Southampton, Southampton, U.K.
and Rutherford Laboratory, Chilton, Oxfordshire, U.K.

## 1. ABSTRACT

It is important to choose the method of solution most appropriate to a particular field problem bearing in mind the type of boundary condition, the field equation and the assumptions which may reasonably be made. A comparison is made of two methods of solving the Laplacian field in the air gap of an electrical machine with slotted boundaries, the two methods under comparison being a numerical conformal transformation[1] and a boundary integral method[2].

An example is given showing flux quantities obtained and also the components of force acting on the stator and rotor teeth for an arbitrary displacement of slotted surfaces. Field solutions of this type are of considerable value in determining the causes of excessive harmonic loss and magnetic noise in induction machines.

## 2. CONFORMAL TRANSFORMATION

The use of conformal transformation is limited to two-dimensional problems and the boundary has to be assumed highly permeable[1] ($\mu = \infty$). However, the treatment of sharp corners presents no difficulty, the numerical evaluation of constants is rapidly convergent and the quantities of interest whether flux quantities, densities or forces can be very conveniently determined. Apart from the possibility of treating complicated boundaries,the appropriate boundary conditions can be 'sewn together', thereby reducing computer time,avoiding non essential variables. Expressions for flux densities are readily developed, and, from these, integrals for Maxwell stresses can be derived.

To show how simply flux quantities and forces can be calculated using conformal transformation, an example is given of the computation of the flux entering induction machine teeth. The tangential and normal components of force acting on a typical stator tooth under load conditions is subsequently determined.

The flux distribution around a complete tooth can be obtained from a combination of the solution of the fields in the three regions, each of which is shown in figure 1. Region 1 contains two displaced slots. It is important to note that the flux in the airgap is almost uniform at points AA' and BB' remote from the slot openings, so that the separate solutions can be combined. Region 2 contains one slot. Again the flux in the airgap is almost uniform at points AA', BB' remote from the slot opening. Region 3 contains no slots and the airgap flux is uniform. Both flux and normal component of force can be calculated easily provided the airgap mmf is known

In Figure 1, the slots are shown as open. Semi-closed slots can be treated using conformal transformation. However, such slots can also be treated more conveniently using the open-slot configuration, with a nominal slot width having a value lying between that of the slot opening and the actual slot width as determined by numerical experiments.

The solution of the fields in the two regions, using conformal transformation, shall now be considered. Region 2 will be treated first as it is the simpler.

### Singly Slotted Boundary

The singly slotted boundary is shown in Figure 2, located in the z-plane, with corresponding points in the t-plane. The well known method of conformal transformation consists of transforming the real axis of the t-plane into the boundary in the z-plane. Since flux is conserved by the transformation, the field is solved in the simpler t-plane region.

The Schwarz-Christoffel transformation equation which transforms the real axis of the t-plane to the boundary in the z-plane is

given by

$$\frac{dz}{dt} = \frac{S\sqrt{(t-c_2)(t-c_3)}}{t(t-1)}$$

By evaluating the residues at the poles of dz/dt, it can be shown that

$$S = 1/\pi$$

$$c_2 c_3 = 1$$

$$c_3 = \frac{(S_2^2 + 2)}{2} + \frac{S_2\sqrt{S_2^2 + 4}}{2}$$

where $S_2$ is the slot width and g, the gap width, is taken as unity.

The transformation equation can be integrated to give z, that is

$$Z = \frac{1}{\pi}\int \frac{\sqrt{(t-c_2)(t-c_3)}}{t\,(t-1)}\,dt \qquad (2.1)$$

This integral can be solved analytically. In the range $|-c_o, -c_1|$ the integrand in equation (2.1) is complex and has to be rearranged as follows

$$Z = \frac{j}{\pi}\int \frac{\sqrt{(c_2-t)(t-c_3)}}{t\,(t-1)}\,dt$$

This integral can now be solved using the transformation

$$p^2 = \frac{c_2-t}{t-c_3}$$

the solution being

$$Z = \frac{2j}{\pi}\left|\tan^{-1} p - \tan^{-1}\frac{p}{c_2} - \frac{(c_2-1)}{2\sqrt{c_2}}\log\frac{\sqrt{c_2}+p}{\sqrt{c_2}-p}\right| \qquad (2.2)$$

for side A and

$$Z = \frac{2j}{\pi}\left|\tan^{-1} p - \tan^{-1}\frac{p}{c_2} + \frac{(c_2-1)}{2\sqrt{c_2}}\log\frac{p-\sqrt{c_2}}{p+\sqrt{c_2}}\right| \qquad (2.3)$$

for side B.

In all other ranges, the integrand is real, and using the transformation

$$p^2 = \frac{t - c_3}{t - c_2}$$

the solution to equation (2.1) is

$$Z = \frac{1}{\pi}\left|\log\left|\frac{1+p}{1-p}\right| - \log\left|\frac{c_3+p}{c_3-p}\right| - \frac{2(c_3-1)}{\sqrt{c_3}}\tan^{-1}\frac{p}{\sqrt{c_3}}\right| \qquad (2.4)$$

Since an induction motor under load conditions is being considered the correct field in the z-plane, requires in the t-plane a point current source of value $I_3$ at t=0 and a point current source of value $I_2$ at t=1. The current $I_2$ is the instantaneous value of current flowing in the conductor in the slot and $I_3$ is the instantaneous value of the airgap mmf in the region of the induction motor where the slot is located. This current represents the effect of the other slots in the machine. The field in the t-plane is given by a function of the form

$$= \frac{1}{\pi}\left(I_3 \log t + I_2 \log (t-1)\right) \qquad (2.5)$$

To obtain the flux entering or leaving a segment of the boundary, the t-plane values corresponding to the points in the z-plane are substituted into the real part of equation (2.5). (Note the imaginery part of this equation gives the potential function).
To obtain the t-plane point corresponding to a point in the z-plane, an equation of the form

$$Z - f(p) = 0 \qquad (2.6)$$

has to be solved, where f(p) is the r.h.s. of either equation (2.2), (2.3) or (2.4). Equation (2.6) can be solved by the bisection method.

Using Maxwell stresses, the force components can be evaluated. For the single and double slot regions this involves integrating $\frac{1}{2\mu_o}\int B^2 dz$ around a suitable contour, and this can be expressed in the present problem as

$$\frac{1}{2\mu_o}\int \left[\frac{dw}{dt}\right]^2 \frac{dt}{dz}\, dt \qquad (2.7)$$

Further the integration can be expressed as a function of t, that is

$$F = \frac{1}{2\mu_o S\pi^2}\int \frac{(I_3(t-1) + I_2 t)^2}{t(t-1)\sqrt{(t-c_2)(t-c_3)}}\, dt \qquad (2.8)$$

The tangential components of force acting on the slot sides can be found by integrating between the limits ($c_2$, $\delta_1$, where $\delta_1 < 1$) and ($\delta_2$, $c_3$, where $\delta_2 > 1$). The choice of $\delta_1$ and $\delta_2$ is made by finding a point z far enough down the slot so that the flux has become uniform.

The uniform flux is, of course, that associated with the current source at t=1 and is the slot leakage flux. It is an easy calculation to find the force contribution associated with this uniform flux.

Using the transform $p^2 = (c_2 - t)/(t - c_3)$ the solution of equation (2.8) is given by

$$F = \frac{j}{\mu_o \pi}\left|(I_2 + I_3)^2 \tan^{-1} p - I_3 \tan^{-1}\frac{p}{\sqrt{c_2}} + \frac{I_2}{2\sqrt{c_2}(1-c_3)} \log\frac{\sqrt{c_2}+p}{\sqrt{c_2}-p}\right|$$

for side A, and

$$F = \frac{j}{\mu_o \pi}\left|(I_2 + I_3)^2 \tan^{-1} p - I_3 \tan^{-1}\frac{p}{\sqrt{c_2}} - \frac{I_2}{2\sqrt{c_2}(1-c_3)} \log\frac{p-\sqrt{c_2}}{p-\sqrt{c_2}}\right|$$

for side B.

The normal components of force acting on the airgap segments of the boundary is obtained using the transformation $p^2 = (t-c_3)/(t-c_2)$ and is given by

$$F = \frac{1}{2\mu_o \pi}\left|(I_2+I_3)^2 \log\left|\frac{1+p}{1-p}\right| - I_3^2 \log\left|\frac{c_3+p}{c_3-p}\right| + \frac{2I_2^2\sqrt{c_3}}{(c_3-1)} \tan^{-1}\frac{p}{\sqrt{c_3}}\right|$$

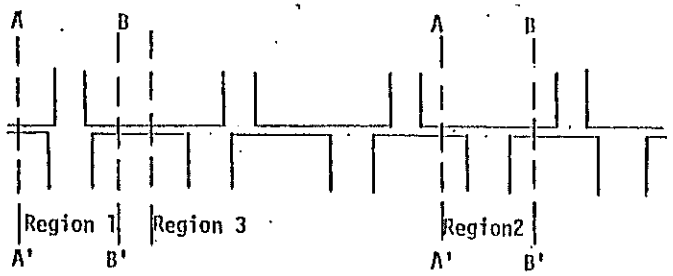


FIGURE 1 : A TYPICAL SECTION OF THE SLOTTED BOUNDARY OF AN INDUCTION MOTOR

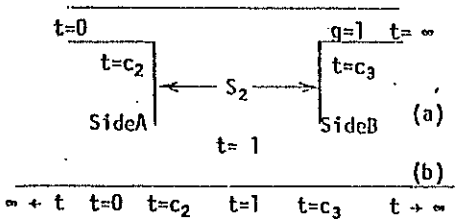


FIGURE 2 : SINGLY SLOTTED BOUNDARY
(a) z-plane
(b) t-plane

Doubly Slotted Boundary

The pair of slots are shown in Figure 3; the boundary shape being located in the z-plane with corresponding points in the t-plane.

The upper slot has a width $S_1$, the lower slot width $S_2$ and $S_2 > S_1$. The gap width is again assumed to be unity. The transformation equation for the doubly slotted boundary is given by

$$\frac{dz}{dt} = \frac{S\sqrt{(t+c_o)\ (t+c_1)\ (t-c_2)\ (t-c_3)}}{t\ (t+1)\ (t-c_4)}$$

where S, $c_o$, $c_1$, $c_2$, $c_3$ and $c_4$ are constants of the equation.

To find the six constants it is necessary to establish six equations. Four of the six equations can be found by evaluating the residues of the poles of dz|dt, and this leads to the following equations

$$S = \frac{1}{\pi} \qquad (2.9)$$

$$c_4^2 = c_o c_1 c_2 c_3 \qquad (2.10)$$

$$S_1(1+c_4)^2 = (c_o-1)(1-c_1)(c_2+1)(c_3+1) \qquad (2.11)$$

and

$$S_2(1+c_4)^2 c_4^2 = (c_4+c_o)(c_4+c_1)(c_4-c_2)(c_3-c_4) \qquad (2.12)$$

These are the only explicit relationships that can be obtained, the others are obtained as follows.

One equation can be obtained from the fact that the two surfaces on either side of the slot are collinear. For the upper slot, in Figure 3, this condition involves evaluating the integral

$$P\left| \int_{-c_1}^{-c_o} \frac{S\sqrt{(t+c_o)(t+c_1)(t-c_2)(t-c_3)}}{t\ (t+1)\ (t-c_4)}\ dt \right| = 0 \qquad (2.13)$$

The other equation involves the slot displacement d, in figure 3, this quantity being related to the transformation equation as follows:

$$d = P \int_{c_o}^{c_2} \frac{S\sqrt{(t+c_o)(t+c_1)(t-c_2)(t-c_3)}}{t(t+1)(t-c_4)}\ dt \qquad (2.14)$$

where P denotes that both integrals have as a limit a Cauchy principle value. Neither integral can be solved analytically and a numerical method has to be used.

Before describing the numerical integration technique, a brief description will be given of the method used in solving the set of non-linear equations.

The set of equations have been solved using numerical optimisation techniques. In particular, direct search methods involving the minimisation of a sum of squares function have been employed. Equations (2.10) - (2.14) are rearranged into the following form

$$f_1 = c_4^2 - c_o c_1 c_2 c_3$$

$$f_2 = S_1(1+c_4)^2 - (c_o-1)(1-c_1)(c_2+1)(c_3+1)$$

$$f_3 = S_2(1+c_4)^2 c_4^2 - (c_4+c_o)(c_4+c_1)(c_4-c_2)(c_3-c_4)$$

$$f_4 = P\left| \int_{-c_1}^{-c_o} \frac{S\sqrt{(t+c_o)(t+c_1)(t-c_2)(t-c_3)}}{t\ (t+1)(t-c_4)}\ dt \right|$$

$$f_5 = d - P \int_{-c_o}^{c_2} \frac{S\sqrt{(t+c_o)(t+c_1)(t-c_2)(t-c_3)}}{t\ (t+1)(t-c_4)}\ dt$$

A function SUM is defined as

$$\sum_{i=1}^{5} (f_i\ (c_o\ c_1,\ c_2,\ c_3,\ c_4,\ t)\ )^2$$

The direct search method varies $c_o$, $c_1$, $c_2$, $c_3$ and $c_4$ until SUM is made sufficiently small.

There are a number of direct search methods available for solving sets of non-linear equations. The authors have used Peckham's[3] method because it requires fewer function evaluations which is clearly an

advantage when evaluating functions which contain definite integrals evaluated numerically. A routine has been written in which the constants can be found for a range of slot displacement.

The solution of Cauchy principal value integrals is the subject of another paper written by some of the present authors[4] and it is clearly not possible to give full details of this work. Only a brief outline of one of the methods used in the solution of equations (2.13) and (2.14) will be given here.

Consider equation (2.13) again in the following form:

$$P \left| \int_{-c_1}^{-c_0} \frac{S\sqrt{(t+c_0)(t+c_1)}}{t} F(t)dt \right| = 0$$

where F(t) is that part of the integrand that is well-behaved in the range $(-c_0, -c_1)$. The range of integration can be transformed to the range (-1, 1) by the linear transformation

$$t = \frac{1}{2}\left[-c_0 - c_1 + x\,(c_1-c_0)\right]$$

Equation (2.13) then becomes

$$P \left| \int_{-1}^{1} \frac{K\sqrt{(1-x)(1+x)}}{x - A} G(x) \right| = 0 \qquad (2.15)$$

where $K = \frac{S(c_1-c_0)}{2}$ , $A = \frac{2-c_0-c_1}{c_0-c_1}$

and G(x) is the transformed function F(t). Since G(x) is a well-behaved function in (-1, 1) it can be expanded as a Taylor series about the point x=A to give

$$G(x) = G(A) + G'(A)(x-A) + \frac{G''(A)(x-A)}{2!} + \ldots$$

If a function M(x) is now defined as

$$M(x) = \frac{G(x) - G(A)}{x - A}$$

it can be seen that

$$M(x) = G'(A) + \frac{G''(A)\,(x-A)}{2!} + \ldots$$

which is also a well-behaved function in (-1, 1). Returning to equation (2.15) this can be rearranged as

$$\left| P \int_{-1}^{1} K \frac{\sqrt{(1+x)(1-x)}}{x - A} G(A)dx + \int K \sqrt{(1+x)(1-x)}\ M(x)dx \right|$$

The first term on the r.h.s is a principal value and can be evaluated analytically. Using the transformation $x = \cos\theta$, it can be shown that the integral is equal to $-KA\pi G(A)$. Again using the transform $x = \cos\theta$, the second integral on the r.h.s. can be simplified and then solved by any standard numerical technique available for solving proper integrals. Equation (2.14) can be treated in a similar manner.

To obtain the correct field in the z-plane, it is necessary to have in the t-plane a current of value $I_3$ at t=0, $I_2$ at $t=c_4$ and $I_1$ at t=-1. Again $I_3$ is the local airgap m.m.f. and $I_1$ and $I_2$ the instantaneous values of current following in the respective conductors of the slots. The field in the t-plane is given by a function of the form

$$w = \frac{1}{\pi} \left| I_3 \log t + I_1 \log(t+1) + I_2 \log(t-c_4) \right| \qquad (2.16)$$

The flux entering or leaving any segment of the boundary may be obtained by evaluating the real part of equation (2.16), substituting the t-plane points corresponding to the points in the z-plane. The value of the t-plane points are found as before by solving the implicit equation

$$z - f'(p) = 0$$

except that f' is, of course, an integral.

Both tangential and normal components of force can be found by evaluating the integral $\frac{1}{2\mu_0}\int B^2 dz$ over a suitable contour.

Using equation (2.7), the force integral becomes

$$F = \frac{1}{2\pi^2\mu_0 S}\int \frac{(I_3(t+1)(t-c_4) + I_1 t(t-c_4) + I_2 t(t+1))^2\, dt}{t(t+1)(t-c_4)\sqrt{(t+c_0)(t+c_1)(t-c_2)(t-c_3)}}$$

The same consideration as to the limits of integration apply in this case as in the singly-slotted boundary. Also the same method of integration is used as that for solving equations (13) and (14).

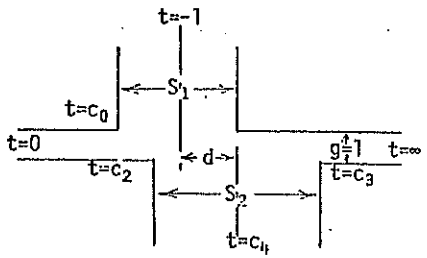


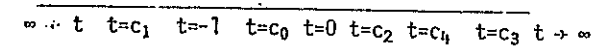


FIGURE 3 : DOUBLY SLOTTED BOUNDARY
(a) z-plane
(b) t-plane

## 3. BOUNDARY INTEGRAL METHOD (B/M)

### Introduction

A number of standard procedures for the solution of magneto-static problems involve discretising the domain of interest into elements and applying the method of finite differences or fininte elements to effect solutions of the appropriate differential or integral equations.

The task of generating a mesh of elements for models having complicated boundaries can lead to difficult data preparation problems and large systems of equations which result in high computational cost. The attraction of conformal transformation is that only the boundaries are specified and also that semi-analytical techniques are used to generate rapid solutions. However, with the development of the boundary integral method, certain constraints necessary to conformal transformation can be removed. For example, problemswithfinite permeability and distributed conductors can be solved by subdividing the boundaries into line elements. By this method, quite complex boundary shapes can be handled relatively economically. The boundary integral method depends upon a direct application of Greens Theorem and has been used for a variety of harmonic problems, [5] including those arising in magnetostatic[2].

### Formulation

The general equations for magnetostatics are as follows:

$$\text{curl } \underline{H} = \underline{J} \qquad (3.1)$$

$$\text{div } \underline{B} = 0 \qquad (3.2)$$

$$\underline{B} = \mu\underline{H} \qquad (3.3)$$

Where $\underline{B}$ and $\underline{H}$ are the magnetic flux density and magnetic field intensity respectively. $\underline{J}$ is the current density and $\mu$ the permeability. If a scalar potential $\phi$ is introduced such that

$$\underline{H} = \nabla\phi + \underline{Hs} \qquad (3.4)$$

$$\text{with curl } \underline{Hs} = \underline{J} \qquad (3.5)$$

then $\nabla^2\phi = 0$ (3.6)

provided $\mu$ is a constant. $\underline{H}s$ is the known excitation field. By application of Greens second theorem to this potential the following boundary integral equation holds.

In two dimensions

$$\phi = \frac{1}{4\pi} \int_S (\log r \frac{\delta\phi}{\delta n} - \frac{\delta}{\delta n} (\log r)\ \phi)\ ds \qquad (3.7)$$

when r is the distance from the source to the field point. Further more, at the interface between two regions the axial continuity conditions hold,

$$\text{i.e. } \mu_1 \frac{\delta\phi}{\delta n} + \mu_1 Hsn = \mu_2 \frac{\delta\phi}{\delta n}_2 + \mu_2 Hsn$$
$$\phi_1 = \phi_2 \qquad (3.8)$$

The boundary integral equation (3.7) can be solved by point collocation if either $\phi$ or $\frac{\delta\phi}{\delta n}$ is known on the boundary. In fact for a well posed problem at least one of these variables must be known. At an interface neither is known, but the continuity equations (3.8) supply the necessary extra information. The algorithm for obtaining the solution requires each boundary and interface to be discretised and the unknown functions ($\phi$ or $\frac{\delta\phi}{\delta n}$) are then found by solving a set of linear equations. The coefficients are determined by analytic quadrature over each boundary facet, see reference 2.

Application to air gap geometry

The problems shown in figures 4 and 5 were solved by this method using 70, 110 and 135 boundary elements. The source fields from the conductors situated at the bottom of the slots were determined analytically. The permeability was conveniently set at 1000 for purposes of comparison with the alternative method. The comparison of the results for the these levels of discretisation used indicated that the errors for the last model (135 elements) is of the order of 1%.

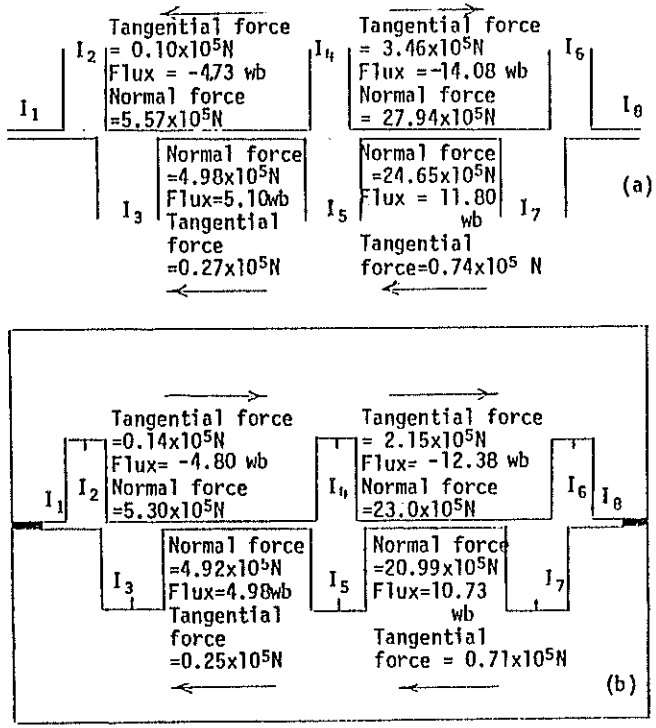


$I_1 = -0.90 \times 10^5$ amps
$I_2 = -3.40 \times 10^5$ amps
$I_3 = 6.36 \times 10^5$ amps
$I_4 = -3.85 \times 10^5$ amps
$I_5 = 6.36 \times 10^5$ amps
$I_6 = -4.30 \times 10^5$ amps
$I_7 = 6.36 \times 10^5$ amps
$I_8 = -6.63 \times 10^5$ amps

FIGURE 4 : THE FIRST PART OF THE AIRGAP PERIPHERY IN WHICH THE AIRGAP FIELD AND FORCE COMPONENTS ARE OBTAINED.
(a) Results obtained using conformal transformation
(b) Results obtained using the boundary integral method

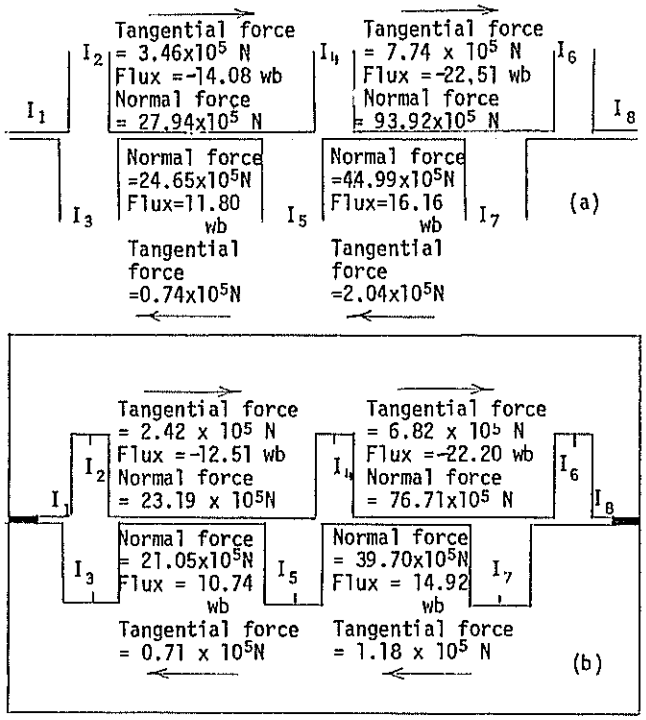


$I_1$ = 2.06 x $10^5$ amps
$I_2$ = -3.85 x $10^5$ amps
$I_3$ = 6.36 x $10^5$ amps
$I_4$ = -4.3 x $10^5$ amps
$I_5$ = 6.36 x $10^5$ amps
$I_6$ = -5.19 x $10^5$ amps
$I_7$ = 6.36 x $10^5$ amps
$I_8$ = -7.8 x $10^5$ amps

FIGURE 5 : THE SECOND PART OF THE AIRGAP PERIPHERY IN WHICH THE AIRGAP FIELD AND FORCE COMPONENTS ARE OBTAINED

(a) Results obtained using conformal transformation

(b) Results obtained using the boundary integral method

## 4. DISCUSSION

The comparison of the two methods reveals interesting aspects regarding assumptions and sources of inaccuracy. When applied to the same boundary shape and conditions, the solutions vary because of the differing sources of inaccuracy. The conformal transformation method does not suffer from discretisation error and the quadrature procedure can be made as accurate as is needed. The technique of treating the boundary in parts can give rise to error but this can be made negligible in all cases by taking two pairs of slots on each side. The assumption of high permeability is, of course, inherent in the method.

By contrast, the boundary integral method can treat finite permeability and can be used in a 3-dimensional problem. However, it is considerably more time consuming and involves a discretisation error.

Results have been obtained by both methods for two slotted configurations with different current levels and boundary displacements. Values of the total flux entering the teeth and the normal and tangential components of forces are computed using both methods. Figures 4 and 5 show typical regions of the air gap field and force components for parts of the air gap periphery.

The differences in flux and force quantities though small are of interest. The use of conformal transformation results in larger tooth fluxes because of the neglect of core reluctance. The boundary integral method is bounded so that core back reluctance and tooth depth could be significant. The boundary integral method inherently involves discretisation and tooth fluxes are computed by integration of field strength. On the other hand the assumption of infinite permeability in the conformal transformation method involves a neglect of core reluctance but gives a very precise representation of the boundary. Discretisation errors in the boundary integral method have to be weighed against the economy of producing a rapid solution. On the other hand the conformal transformation method involves very low inherent error

within the assumption of high permeability. A typical ratio of time for computing a problem of the kind discussed here would be 100 : 1 in favour of conformal transformation. It must be borne in mind, however, that the boundary integral method has wider scope.

## REFERENCES


1. BINNS, K. J. and LAWRENSON, P. J. : 'Analysis and computation of electric and magnetic field problems', Pergamon, 1973.

2. SIMKIN, J. and TROWBRIDGE, C. W. : 'Magnetostatic fields computed using an integral equation derived from Green's theorem, Proc. Compumag, Oxford, 1976.

3. PECKHAM, G. : 'A new method for minimising a sum of squares function without calculating gradients', Computer J., 1970, Vol. 13, pp 418-420.

4. BINNS, K. J., ROWLANDS-REES, G and KAHAN, P. A. : 'The evaluation of improper integrals encountered in the use of conformal transformation', Int. J. for Num. Methods in Engineering (to appear shortly).

5. JAWSON, M. A. : 'Integral Equation Methods in Potential Theory I', Proc. Roy. Soc. A., 275, 23-32, 1963.

# A MONTE CARLO METHOD FOR SURFACE FIELD CALCULATIONS

J.H. Pickles
Central Electricity Research Laboratories,
Leatherhead, Surrey, KT22 7SE, England

## ABSTRACT

A Monte Carlo method for the solution of Laplace's equation in complicated geometries is outlined. The method relies on the use of 'floating' random walks. These are random walks defined and constructed independently of any particular grid or co-ordinate system. Applications to the calculation of electrostatic potentials and fields are described. A modified method, appropriate to the calculation of fields at boundary surfaces, is presented. Finally, reference is made to the use of the floating random walk approach for the solution of other partial differential equations.

## 1. INTRODUCTION - THE FLOATING RANDOM WALK METHOD

It has long been known that the solution of some partial differential equations can be translated into Monte Carlo problems concerning the motion of random walks. The earliest, and best known example, is the method of Courant et al.[1] for the solution of Laplace's equation. Consider a potential $\phi$ specified on the boundary B of some region R and satisfying Laplace's equation within it. Suppose that a finite difference grid is superimposed on R and that it is desired to evaluate $\phi$ at some grid point $\underline{r}_o = (x_o,y_o,z_o)$. Then $\phi(\underline{r}_o)$ can be estimated from the properties of a family of random walks which start at $\underline{r}_o$ and move randomly from grid point to grid point until they reach the boundary. The Laplacian property of the potential $\phi$, as expressed on a grid of spacing h,

$$\phi(x,y,z) = \frac{1}{6}\{\phi(x+h,y,z) + \phi(x-h,y,z) + \phi(x,y+h,z) + \phi(x,y-h,z) + \phi(x,y,z+h) + \phi(x,y,z-h)\}$$

translates, as far as the behaviour of the random walks is concerned, into the equal probabilities of 1/6 for the allowed steps $(x,y,z) \to (x\pm h,y,z), (x,y\pm h,z), (x,y,z\pm h)$. It is found that with a family of n random walks, which reach the boundary, where $\phi$ is known, at points $\underline{r}_1^*,\ldots,\underline{r}_n^*$

$$\phi(\underline{r}_o) \simeq \frac{1}{n}\sum_{i=1}^{n}\phi(\underline{r}_i^*) \qquad (1)$$

The accuracy of the estimate of $\phi(\underline{r}_o)$ increases with the number of random walks n.

This approach, though interesting, turns out to be rather impractical, because of the very large computational effort needed for the construction of the random walks. Conventional methods for the solution of the original Laplace problem are far more efficient[2]. A more effective random walk method is obtained if one disposes of the superfluous notion of the grid. The Laplacian property of the potential can be expressed more fundamentally by the mean value theorem of potential theory. If $\underline{r}$ is a point within R, and S a sphere centred at $\underline{r}$, of radius a, which lies wholly within R

$$\phi(\underline{r}) = \frac{1}{4\pi a^2}\int_{S_o}\phi(\underline{r}')\,dS' \qquad (2)$$

The potential at the centre of the sphere is equal to the average of the potentials $\phi(\underline{r}')$ taken over its surface. Translated into the random walk approach[3,4], the mean value theorem allows a walk which has reached $(x,y,z) \equiv \underline{r}$ to travel in one step from $\underline{r}$ to a point chosen randomly on the surface of the sphere S. S may in particular be chosen to be the sphere centred at $\underline{r}$ which just touches the boundary B; the step length from $\underline{r}$ is thus equal to the distance from $\underline{r}$ to the nearest point on B. Walks proceed by a succession of such steps, as shown in Fig. 1, terminating when they are sufficiently close to the boundary. The potential at their starting point $\underline{r}_o$ is estimated as before, by averaging over random walks as in equation (1). The computational advantage of these 'floating' random walks, as they are called, is that they reach the boundary and terminate in fewer steps than the grid-based 'fixed' random walks.

Monte Carlo calculations with floating random walks are, accordingly, much quicker, but there remains the apparent difficulty that a separate set of random walks is needed to calculate the potential of each point $\underline{r}_o$ of interest in the region $R_o$. Again, improvement is possible. The information contained, not only in the potential $\phi(\underline{r}_i^*)$ of the point where a walk terminates, but in its path from $\underline{r}_o$ to $\underline{r}_i^*$, must be exploited. In particular, the direction of its first step, from $\underline{r}_o$ to some point $\underline{r}_{1i}$ on the surface of the sphere $S_o$ in Fig. 1, contains useful information[5]. From the potential theory point of view, if $\underline{r}_p$ is a general point within $S_o$,

$$\phi(\underline{r}_p) = \int_{S_o}\phi(\underline{r}')\,\frac{\partial G(\underline{r}_p,\underline{r}')}{\partial n}\,dS' \qquad (3)$$

where $G(\underline{r},\underline{r}')$ is the Green's function for the sphere defined so that $G(\underline{r},\underline{r}') = 0$ when $\underline{r}$ or $\underline{r}'$ lies on $S_o$. In terms of random walks, equation leads to the estimate of the potential $\phi(\underline{r}_p)$

$$\phi(\underline{r}_p) = \frac{1}{n}\sum_{i=1}^{n} W(\underline{r}_p,\underline{r}_o,\underline{r}_{1i})\,\phi(\underline{r}_i^*) \qquad (4)$$

where the weighting factors $W(\underline{r}_p,\underline{r}_o,\underline{r}_{1i})$ are determined from the Green's function. If $S_o$ has radius $a_o$,

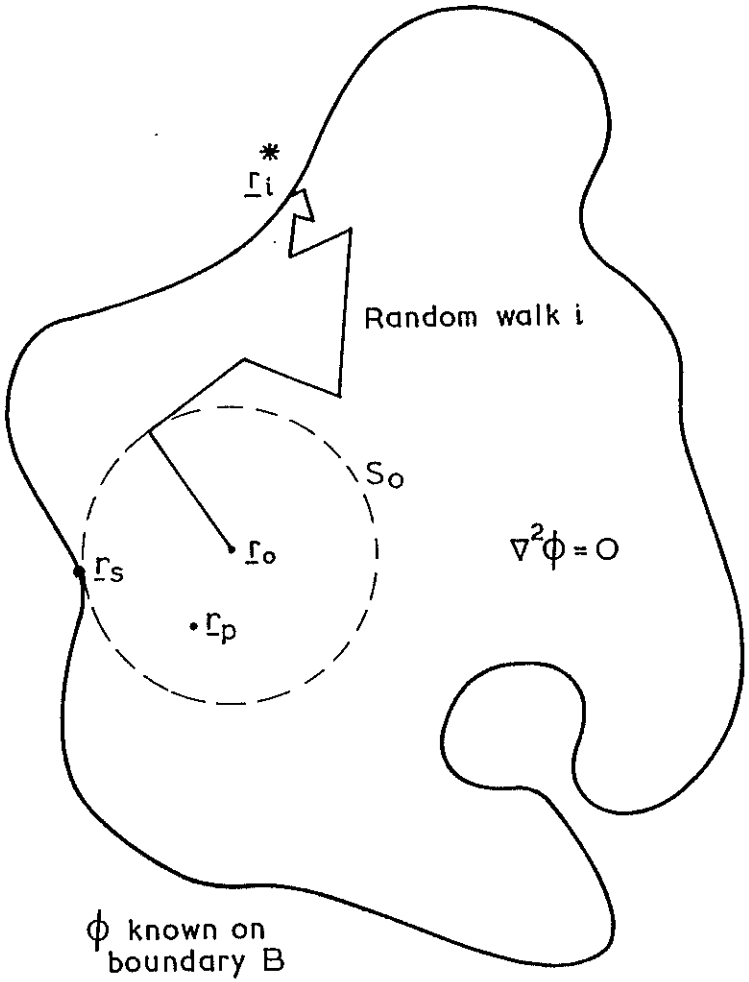


FIG. 1 PATH OF A FLOATING RANDOM WALK

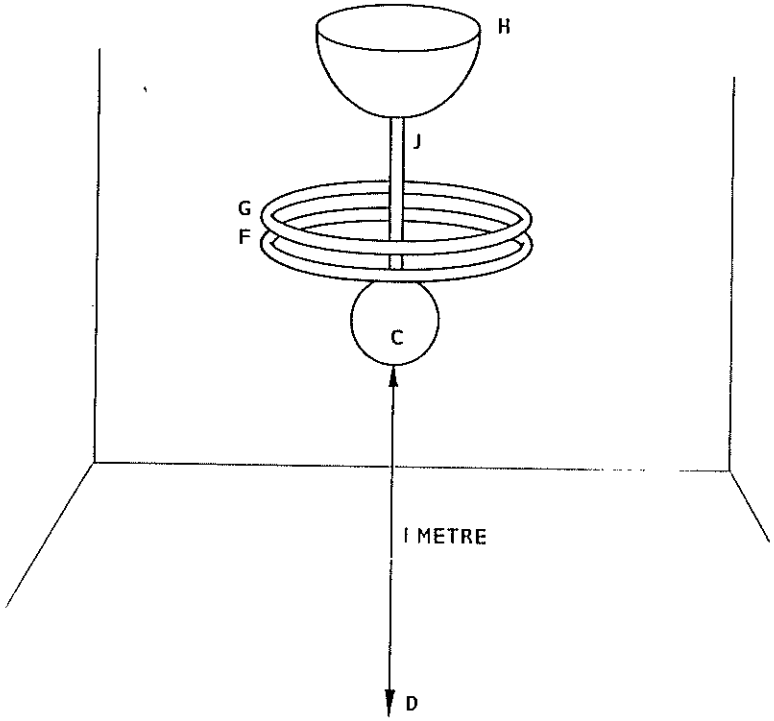


FIG. 2 GEOMETRY OF SPHERE - PLANE GAP

$$W(\underline{r}_p,\underline{r}_o,\underline{r}_{1i}) = 4\pi a_o^2 \frac{\partial G(\underline{r}_p,\underline{r}_{1i})}{\partial n} = \frac{a_o(a_o^2 - |\underline{r}_p - \underline{r}_o|^2)}{|\underline{r}_p - \underline{r}_{1i}|^3} \qquad (5)$$

Equation (1) has been generalised to a weighted average representation which, with weights specified by equation (5), estimates the potential at all points $\underline{r}_p$ within the sphere $S_o$. Estimates of fields, $-\nabla\phi(\underline{r}_p)$, follow from a direct analytical differentiation:

$$-\nabla\phi(\underline{r}_p) \simeq -\frac{1}{n}\sum_{i=1}^{n} \nabla W(\underline{r}_p,\underline{r}_o,\underline{r}_{1i})\ \phi(\underline{r}_i^*) \qquad (6)$$

## 2. APPLICATION TO ELECTROSTATIC PROBLEMS

The procedure described above has been made the basis of a general purpose computer program for solving Laplace's equation in high voltage electrostatic applications. For the purposes of calculation and data input a modular representation of the boundary is adopted. It is regarded as built up, by juxtaposition and superposition, of combinations of suitable elementary surfaces (rod, box, sphere, torus, etc.). Then the distance from any point $\underline{r}$ to each of the elementary surfaces (e.g. a box) can be expressed as an analytic function (e.g. of $\underline{r}$ and the co-ordinates of the corners of the box). For a random walk which has reached a point $\underline{r}$, the appropriate expressions for the distances to each of the elementary surfaces are evaluated, the smallest such distance determining the length of the next step. In this way the effects on electric fields of the complicated geometries of, say, transmission towers or transformers, are measured by their influence on the paths of the random walks; they do not need to be explicitly 'thought out'. Electric fields accurate to within 2-3% can readily be obtained in practice. For example, the calculation of potentials and fields along the line of the sphere-plane gap CD in Fig. 2 required 1200 random walks and a c.p.u. time of 19.5 s on an IBM 370/168 computer. Details (including an account of the use of a crude initial approximation to increase further the efficiency of the Monte Carlo calculation) are given in Reference 5.

## 3. SURFACE FIELD CALCULATIONS

One of the weaknesses of the floating random walk method described in Section 1 is that it is difficult to estimate fields at points on the boundary, for example on the sphere surface C of Fig. 2. This is a serious weakness because surface fields are often of particular physical interest. The reason for the difficulty can be seen by going back to equation (3). This is valid only for points $\underline{r}_p$ within the sphere $S_o$; for the point $\underline{r}_s$ where $S_o$ touches the boundary B, it is, so to speak, only marginally valid. It is found that in consequence the weights $W(\underline{r}_s,\underline{r}_o,\underline{r}_{1i})$ and $\nabla W(\underline{r}_s,\underline{r}_o,\underline{r}_{1i})$ in the estimates (4) and (6) become very large for random walks with $\underline{r}_{1i}$ close to $\underline{r}_s$. In particular, the statistical sampling variance of the Monte Carlo estimate (6) for $\nabla\phi(\underline{r}_s)$ diverges. The difficulty occurs, clearly, whatever the choice of $\underline{r}_o$, the centre of the sphere $S_o$, so that no valid estimate of the surface field $-\nabla\phi(\underline{r}_s)$ can be obtained.

The physical meaning of this mathematical difficulty is illustrated in Figs. 3a and 3b. The mathematics of equation (3) is quite general, and no distinction is made between case (a), when the field has a singularity at $\underline{r}_s$, and case (b), when it does not. To get satisfactory estimates of surface fields, some explicit statement regarding the smoothness of the boundary must be introduced. One way in which this can be done is to specify a distance d, as shown in Fig. 3b, over which the potential may be approximated as varying linearly. d contains the physical information implicit in the choice of the grid size in a finite difference calculation.

This requirement on the smoothness of the potential must now be translated into an equivalent rule governing the behaviour of the random walks. Consider a random walk which after its first step reaches a point $\underline{r}_1$ close to B. Let the nearest point on B be $\underline{r}_1^B$, with $|\underline{r}_1 - \underline{r}_1^B|$ less than the 'smoothing distance' d. The assumed linearity of the potential near the boundary can then be exploited by requiring that the walk moves on its second step to a point

$$\underline{r}_2 = \underline{r}_1^B + \frac{d}{|\underline{r}_1 - \underline{r}_1^B|}(\underline{r}_1 - \underline{r}_1^B)$$

before resuming its usual random motion. The bias introduced by this 'compulsory' step is now compensated for by re-writing the estimate of the potential (equation (4)) as

$$\phi(\underline{r}_p) \simeq \phi(\underline{r}_s) + \frac{1}{n}\sum_{i=1}^{n} \nabla(\underline{r}_p,\underline{r}_o,\underline{r}_{1i}) \times$$

$$\left\{\frac{|\underline{r}_{1i} - \underline{r}_{1i}^B|}{d}(\phi(\underline{r}_i^*) - \phi(\underline{r}_s)) + (1 - \frac{|\underline{r}_{1i} - \underline{r}_{1i}^B|}{d})(\phi(\underline{r}_{1i}^B) - \phi(\underline{r}_s))\right\}$$

The field is estimated by differentiation as before:

$$-\nabla\phi(\underline{r}_p) \simeq \frac{1}{n}\sum_{i=1}^{n} \nabla W(\underline{r}_p,\underline{r}_o,\underline{r}_{1i}) \times$$

$$\left\{\frac{|\underline{r}_{1i} - \underline{r}_{1i}^B|}{d}(\phi(\underline{r}_i^*) - \phi(\underline{r}_s)) + (1 - \frac{|\underline{r}_{1i} - \underline{r}_{1i}^B|}{d})(\phi(\underline{r}_{1i}^B) - \phi(\underline{r}_s))\right\} \qquad (7)$$

In equation (7) the factors $|\underline{r}_{1i} - \underline{r}_{1i}^B|/d$ and $(\phi(\underline{r}_{1i}^B) - \phi(\underline{r}_s))$ are small for walks with $\underline{r}_{1i}$ close to $\underline{r}_s$, and so help to smooth their

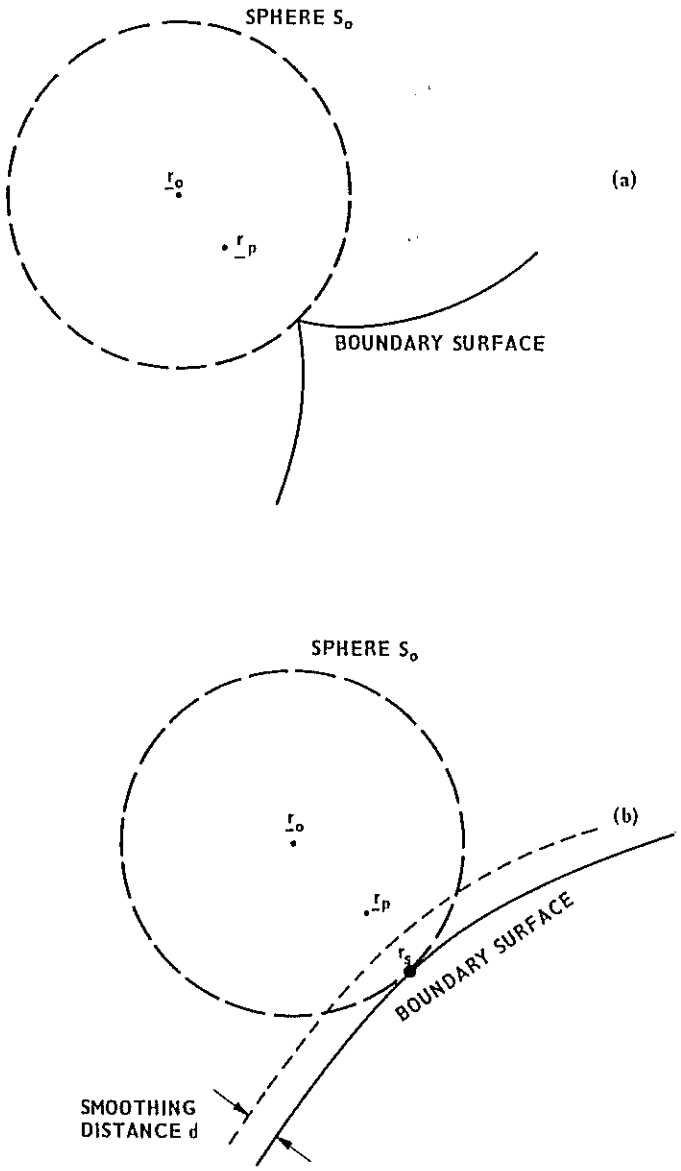


FIG. 3 BOUNDARY GEOMETRIES

large and erratic contributions to the estimated surface field $-\nabla\phi(\underline{r}_s)$.

It turns out, unfortunately, that the field estimate of equation (7) is not yet wholly satisfactory. The divergence in the sampling variance for $\nabla\phi(\underline{r}_s)$, though weaker than for equation (6), remains. Further smoothing is needed, and may be provided by the Monte Carlo technique of importance sampling[2]. The idea is to direct a greater proportion of random walks, with a correspondingly reduced statistical weight, towards the region near $\underline{r}_s$ which is responsible for the divergence. The dependence of the estimate $\nabla\phi(\underline{r}_s)$ on any individual walk is weakened, and its reliability increased. The optimum distribution of random walks for this purpose is found by minimising the expected sampling variance for the surface field, which, computed by standard probability theory, is

$$\sigma^2\left[\nabla\phi(\underline{r}_s)\right] = -\frac{1}{n}\left[\nabla\phi(\underline{r}_s)\right]^2 + \frac{1}{4\pi a_o^{\,2} n}\int_{S_o}\left\{\frac{(\nabla W(\underline{r}_s,\underline{r}_o,\underline{r}_1))^2}{4\pi a_o^{\,2}\, p(\underline{r}_1)}\right.$$

$$\left.\times\left[\frac{|\underline{r}_1 - \underline{r}_1{}^B|}{d}\,(\phi(\underline{r}_i{}^*) - \phi(\underline{r}_s)) + (1-\frac{|\underline{r}_1 - \underline{r}_1{}^B|}{d})(\phi(\underline{r}_1{}^B) - \phi(\underline{r}_s))\right]^2\right\} dS \qquad (8)$$

In equation (8) $p(\underline{r}_1)$ is the probability density for the selection of a walk with a first step $\underline{r}_o \to \underline{r}_1$, and satisfies the constraint

$$\int_{S_o} p(\underline{r}_1)\; dS = 1$$

If the boundary near $\underline{r}_s$ is approximated by a planar surface at a constant potential, the expression (8) becomes analytically tractable and the optimum $p(\underline{r}_1)$ may be found by an application of the calculus of variations[6]. Thus

$$p(\underline{r}_1) = \frac{1}{4\pi\sqrt{2}a_o^{\,2}}\left(\frac{a_o}{a_o - (\underline{r}_1 - \underline{r}_o)\cdot(\underline{r}_s - \underline{r}_o)/a_o}\right)^{\frac{1}{2}} \qquad (9)$$

Potential and field estimates, appropriate to the use of a family of random walks whose first steps are biased according to equation (9), can now be obtained. The specific expression for the estimated field is

$$-\nabla\phi(\underline{r}_p) \simeq -\frac{1}{n}\sum_{i=1}^{n}\frac{1}{4\pi a_o^2\, p(\underline{r}_{1i})}\times VW(\underline{r}_p,\underline{r}_o,\underline{r}_{1i})\times$$

$$\left\{\frac{|\underline{r}_{1i}-\underline{r}_{1i}{}^B|}{d}\left(\phi(\underline{r}_1{}^*)-\phi(\underline{r}_s)\right)+\left(1-\frac{|\underline{r}_{1i}-\underline{r}_{1i}{}^B|}{d}\right)\left(\phi(\underline{r}_{1i}{}^B)-\phi(\underline{r}_s)\right)\right\} \qquad (10)$$

Equation (10) applied to the calculation of the surface field $\nabla\phi(\underline{r}_s)$ gives satisfactory results with a finite sampling variance.

The field estimate of equation (10) requires only the construction of the random walks and the evaluation of analytical expressions for the factors $VW(\underline{r}_p,\underline{r}_o,\underline{r}_1)$, $p(\underline{r}_1)$, and $|\underline{r}_1-\underline{r}_1{}^B|/d$. Like equation (6), it is well suited to computer calculations. Two practical tests have been carried out. The first is for the case of a parallel plate condenser, where, of course, the field is known to be uniform. The simplicity of the geometry allows sampling variances to be calculated a priori and used to check those found by numerical experiment. Figure 4 shows both 'theoretical' and 'experimental' sampling variances for the fields calculated by the standard floating random walk method (equation (6)) and the smoothed method (equation (10)). The superiority of the smoothed method at the boundary is clearly shown. The second test is for the more realistic geometry of Fig. 2. In Ref. 5, fields along the sphere-plane gap CD were calculated and the surface field at the sphere C estimated by extrapolation. Here, the smoothed method was employed, with a smoothing distance d of one tenth of the radius of the sphere. Results for the fields at and near the surface were obtained, which were comparable in speed and accuracy with the previous estimates of the fields elsewhere in the gap. 300 random walks and 4.6 s c.p.u. time were needed. Some representative results are given in Table 1.

## 4. FURTHER APPLICATIONS

The random walk methods described here have been developed with electrostatic applications in mind. It would be misleading to suggest that they could be directly applied, without any adaptation, to magnetic problems. Rather, they are presented as examples of what seems generally to be a promising line of study. It may be useful to conclude by listing applications of floating random walk methods which have been suggested for problems beyond the Laplace-equation/Dirichlet-boundary-condition considered here. Some of these are discussed in Ref. 7. For example, Neumann boundary conditions can be handled by the use of boundaries which reflect rather than absorb the random walks. In a similar way materials of different permittivity (or permeability) could be allowed for by imposing the appropriate balance between reflection and transmission of random walks across the dielectric interfaces. Applications to the solution of Poisson's equation seem to be straightforward. The random walks can here be geometrically identical to those used for solving Laplace's equation;

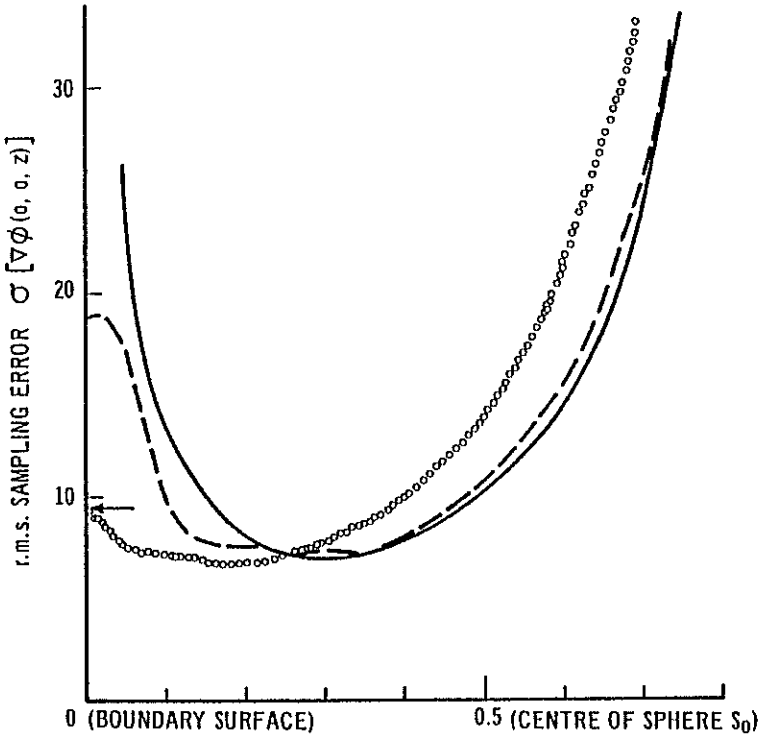


FIG. 4 EXPERIMENTAL AND THEORETICAL ESTIMATES OF SAMPLING ERROR

——— DENOTES THEORETICAL SAMPLING ERROR OF STANDARD METHOD

– – – DENOTES EXPERIMENTAL SAMPLING ERROR OF STANDARD METHOD

oooooooooo DENOTES EXPERIMENTAL SAMPLING ERROR OF MODIFIED METHOD

◄—— DENOTES THEORETICAL LIMITING VALUE AT Z = 0 OF SAMPLING ERROR OF MODIFIED METHOD

| | Modified method (equation (10)) using 300 random walks | | Reference 5 (equation (6)) using 1200 random walks | |
|---|---|---|---|---|
| Distance from sphere C | Estimated field $-\nabla\phi$ (arbitrary units) | r.m.s. sampling error in $\nabla\phi$ | Estimated field $-\nabla\phi$ (arbitrary units) | r.m.s. sampling error in $\nabla\phi$ |
| 0 | 842 | 20 | - | - |
| 0.01 | 638 | 13 | 629 | 17 |
| 0.02 | 511 | 6.1 | 518 | 9.0 |
| 0.05 | 322 | 6.3 | 313 | 6.1 |
| 0.10 | | | 203 | 1.9 |
| 0.15 | | | 152 | 1.0 |
| 0.20 | | | 123 | 0.9 |
| 0.30 | | | 90.1 | 0.7 |
| 0.50 | | | 58.9 | 0.6 |
| 0.75 | | | 42.7 | 0.4 |
| 1.00 (ground at D) | | | 37.7 | - |

Table 1. Field Calculation for the Sphere Plane Gap CD of Fig. 2



only the scoring system in the estimation of potentials needs to be changed, to allow for the inclusion of a charge density term in equations (2) and (3). Time dependent diffusion or heat conduction problems are treated, again with the same random walks, by associating a time increment with each step of a random walk. For these and similar problems the random walk approach could prove useful in tackling geometrically complex problems.

## 5. ACKNOWLEDGEMENT

The work described here was carried out at the Central Electricity Research Laboratories and is published by permission of the Central Electricity Generating Board.

## 6. REFERENCES

1. Courant, R, Friedrichs, K and Lewy, H. Uber die partiellen Differenzengleichungen der Mathematischen Physik. Math. Ann. 100 32-74, 1928.

2. Hammersley, J M and Handscomb, D C.'Monte Carlo Methods' (Methuen 1964).

3. Brown, G W. 'Monte Carlo Methods' in Beckenbach, E F. (Ed.) 'Modern Mathematics for the Engineer'. (McGraw-Hill, 1958).

4. Muller, M E. 'Some continuous Monte Carlo methods for the Dirichlet problem'. Ann. Math. Stat. 27 569-583, 1956.

5. Pickles, J H. 'Monte Carlo field calculations'. Proc. IEE, 124 1271-1276, 1977

6. Pickles, J H. 'Monte Carlo calculations of potential gradients near boundary surfaces'. Central Electricity Research Laboratories Report, RD/L/N 202/76. 1976

7. Haji-Sheikh, A and Sparrow, E M. 'The solution of heat conduction problems by probability methods'. Trans. ASME, C-89, 121-131, 1967.